Politecnico di Torino

ScuDo
Scuola di Dottorato ~ Doctoral School
WHAT YOU ARE, TAKES YOU FAR

Doctoral Dissertation

Nonlinear numerical analysis of thermal buckling and post-buckling of rectangular FG plates with temperature-dependent properties using CUF

By

Majid Afzali

******

Supervisors:

Prof. Erasmo Carrera

Prof. Mojtaba Farrokh

Doctoral Examination Committee:

Prof. Ali Hosseini Kordkheili, Referee, Sharif University of Technology, Iran
Prof. Majid Jamal Omidi, Referee, Malek Ashtar University of Technology, Iran
Prof. Mohammad Reza Khalili, Referee, K.N.Toosi University of Technology, Iran
Prof. Calogero Orlando, Referee, University of Enna Kore, Italy
Prof. Mahnaz Zakeri, Referee, K.N.Toosi University of Technology, Iran

Politecnico di Torino
2023

Declaration

I hereby declare that, the contents and organization of this dissertation constitute my own original work and does not compromise in any way the rights of third parties, including those relating to the security of personal data.

Majid Afzali
2023

* This dissertation is presented in partial fulfillment of the requirements for **Ph.D. degree** in the Graduate School of Politecnico di Torino (ScuDo).

I would like to dedicate this dissertation to my beloved wife Sajdeh, who encouraged me during my Ph.D. program and is by my side at every stage of life. Also, I dedicate it to my dear parents who have been the origin of my support.

Acknowledgements

I would like to many thank my Polito supervisor, Professor Erasmo Carrera, who is a scientist with ethics and ever cooperated with me throughout the Ph.D. duration in the progress of my thesis and articles. I also would like to express my special appreciation to my KNTU supervisor, Professor Mojtaba Farrokh, who has been a tremendous mentor to me and supported me in the advancement of the dissertation with his guidance.

Abstract

The current study is presented to investigate the thermal buckling and post-buckling response of functionally graded (FG) plates with temperature-dependent properties. Constituent properties depend not only on the thickness direction variable but also on temperature. Therefore calculation of the temperature distribution through the thickness is extremely significant. In this regard, an improved method is introduced for determining temperature distribution. Two types of uniform and nonuniform temperature distribution within the thickness are applied to the plate as thermal loads. Here, FEM is used to analyze the thermal buckling and post-buckling problem based on Carrera Unified Formulation (CUF), a powerful formulation and higher-order deformation theory for modeling the plate. In this regard, the nonlinear equilibrium equations are extracted using the virtual work principle by considering large displacements and Green-Lagrange strain. The solution to the problems in this thesis is divided into three general parts: First part is related to calculating the critical thermal buckling load of the FG plate with temperature-dependent properties using linear buckling analysis (LBA). The second part includes a nonlinear thermal post-buckling analysis of the FG plate using the arc-length method. The third part explains the procedure of analyzing the nonlinear thermal post-buckling behavior of the FG plate, considering temperature-dependent properties. In order to validate and prove the accuracy and effectiveness of the current method, several numerical examples are provided to show more precise results than similar references. In addition, some sensitivity analyses are executed to clarify the effects of the volume fraction index, the geometry aspect ratio and thickness of the plate, the order of expansion functions, the type of FGM combination, boundary conditions, temperature-dependent and temperature-independent properties on the thermal buckling load and thermal post-buckling path. The results prove the effectiveness of using CUF on thermal buckling and post-buckling of FG plates. It is illustrated that if temperature-dependent properties are utilized, the results will be more accurate than those without temperature

dependency. One significant result is that in a fully simply supported plate, it can not be seen the bifurcation point in the thermal post-buckling path, while it will be seen in the plate with fully clamped boundary condition.

Keywords: FG plate, Temperature-dependent properties, CUF, Geometrically nonlinear analysis, Thermal buckling and post-buckling, Expansion function

Contents

List of Figures

List of Tables

Chapter 1

Introduction

1.1 Overview

Today, composite plates are used to apply in industries such as Aerospace, Mechanical, and Civil due to their lightweight, high strength, and proper thermal properties. Some researchers have specifically shed light on new types of composite materials known as functionally graded materials (FGM). FGM is a combination of ceramic and metal materials, whose physical properties are defined as a function of both material properties that vary smoothly and continuously from one surface to the other. Nowadays, FGM is used in quite a few structures, like the space shuttle. Since FGM has high temperature resistance and high strength, it is applied to the surfaces of the shuttle. One side of the shuttle's combustion chamber works at very high temperatures while the other side operates at low temperatures because of cool liquid hydrogen [8]. So FGM is a suitable material to resist enormous temperature differences due to thermal stress. In higher temperatures, plates are buckled even with the absence of mechanical loads. Buckling is considered an adverse phenomenon that is likely to damage plates. Thus, designers should investigate to find an accurate method for thermal buckling and post-buckling of the FG plates to prevent failure and damage.

1.2 FGM Utilization

FGMs are widely used in thermal insulation coating for turbine blades, thermoelectric generators, aerospace industries in the surface of aircraft or spacecraft and some parts of space shuttle's motor, biomedical materials including bone and dental implants, automobile manufacturing, electromagnetic industries, sensors, ceramic motors, sports equipment, metal plastics, joining non-isotropic metals, metals with diamond structure, metal plastics reinforced with carbon, etc [9–12].

1.2.1 Description of FGM usage in some industries

More details about the use of FGM in various industries are given as follows:

1. Aerospace: FGMs are extensively used in the aerospace industry due to their ability to withstand extreme conditions by adjusting the material composition from one side to another. They can be employed in aircraft structures, such as wings or fuselages, to optimize their mechanical properties, also in engine components and thermal protection systems. The graded composition of FGMs helps minimize thermomechanical stress concentrations and thermal mismatch, enhancing these structures' overall performance and durability.

2. Biomedical Engineering: FGMs have significant potential in the field of biomedical engineering. They can be utilized in implants, prosthetics, and dental materials. By creating a gradual transition between the implant and the surrounding bone, FGMs can reduce stress concentration and improve the long-term stability of implants. Additionally, FGMs can be designed to have biocompatible surfaces, promoting tissue integration and minimizing rejection risks.

3. Energy Generation: FGMs can be employed in various energy generation systems, such as thermoelectric devices and fuel cells. By tailoring the material properties to optimize thermal conductivity and electrical resistivity, FGMs can enhance energy conversion efficiency. They can also withstand high temperatures and chemical corrosion, making them suitable for use in harsh environments.

4. Automotive and Transportation: FGMs applications can be seen in the automotive and transportation industries. They can be utilized in components like engine parts, brake discs, and exhaust systems, where high temperature resistance and mechanical strength are crucial. FGMs can provide improved performance, reduced weight, and increased fuel efficiency compared to conventional materials.

5. Civil Engineering: FGMs have the potential to enhance the structural integrity of buildings and infrastructure. By designing materials with a gradual change in properties, FGMs can reduce stress concentrations at interfaces and joints. They are employed in bridges, pipelines, and offshore platforms, among other applications.

6. Electronics: FGMs have promising applications in the electronics field. They can be used in electronic packaging to manage heat dissipation by gradually transitioning from materials with high thermal conductivity to insulating materials.

7. Optics: FGMs can be utilized in optical devices to achieve refractive index gradients, enabling better light transmission and reducing reflection losses.

8. Machine tools: In shaping tools, since the consumable materials that are used become harder every day, more advanced tools are needed for cutting and forming them. In this field, compatibility is needed between coating resistance and toughness for the materials of cutting and shaping tools, so the use of FGM in this field is essential. In addition, heat-resistant materials are needed for dry cutting since does not use a cooling fluid; such material has already been made, the outer coating of which is made of diamond and the inside of which is made of steel. With this situation, it is expected that fast-cutting tools will be made soon, without limitations in various shapes and sizes.

Generally, the utilization of FGMs spans a wide range of industries and applications. Their unique properties and versatility make them valuable for improving performance, durability, and efficiency in various fields of engineering and technology.

1.2.2 The capability of FGM to improve characteristics of components

The most important application of FGM is to improve the mechanical or thermal, or thermomechanical characteristics of components in the following manners [9–12]:

1. The amount of thermal stress can be minimized and also, the critical areas where the maximum thermal stress occurs can be controlled.
2. The onset of plastic yielding and failure for a thermodynamic loading can occur with a delay.
3. The resistance of the interface between non-homogeneous solids such as metal and ceramic can be increased by continuously decreasing the composition or changing the direction of mechanical properties.
4. Crack growing can be reduced by choosing the appropriate grading of mechanical properties.
5. Placing the hard coating on the soft sample can be made easier by grading of mechanical properties and directing the change of material properties.
6. The grading of the composition in the surface layers can eliminate the singular fields caused by cutting and sharp tip depressions and changes the plastic deformation characteristics around the depressions.
7. At the connection of two different materials, instead of directly joining two different materials, a layer of FGM is placed between them, which makes the change of properties more smooth.
8. These materials are used as a resistant coating layer in gears, cams, ball and roller bearings in order to reduce the effects of abrasion in machine tools. These layers are made so that their thermal conductivity is high.

1.3 The unique characteristic of FGM

FGM is microscopically nonhomogeneous and its mechanical properties continuously change from one side of the structure to the other. These material changes are

created gradually by changing the volume fraction ratio of two materials. Usually, these materials are made of ceramic and metal. Due to its low heat transfer coefficient and high resistance to temperature, the ceramic structural material tolerates very high temperatures and the metal structural material provides the necessary flexibility. Because of continuous changes in mechanical properties, the continuity troubles that exist in composite structures do not occur in FGM. The bold advantage of using these materials is that they are able to withstand high temperatures.

1.4 Problem Definition

FGM is a type of composite material whose properties are gradually changed through spatial coordinate. These gradual changes in the properties of FG plates make a notable exception in comparison with laminated composites. In laminated composites, the sudden change in the property from one layer to another layer may cause intensive stress in the structure. Thus, employing FGM results in softening this difficulty. In Fig. 2.1, an FG plate is demonstrated.

FGMs, in common, are produced from a combination of two types of materials such as ceramic and metal so as to make an optimum equilibrium between mechanical and thermal properties. High thermal strength and low thermal conductivity of ceramics and great strength of metals are of significant properties of these two types of materials.

In this study, an FG plate with a length of a and width of b and thickness of t is considered for buckling and post-buckling analysis. Many types of ceramic and metal combinations can be used as materials for the FG plate. Some of them that have been used in this study are listed in section 2.3 of chapter 2.

For analysis of FG plates, researchers have utilized theories like classical plate theory (CPT), first-order shear deformation theory (FSDT), and higher-order shear deformation theory (HSDT) with some limitations and simplifications. But, in recent years, to increase the accuracy of the former theories, Carrera Unified Formulation (CUF) has been introduced for the modeling and analysis of beams, plates, and shells [13]. However, up to now, CUF has not been employed for thermal post-buckling analysis of FG plates with temperature-dependent properties.

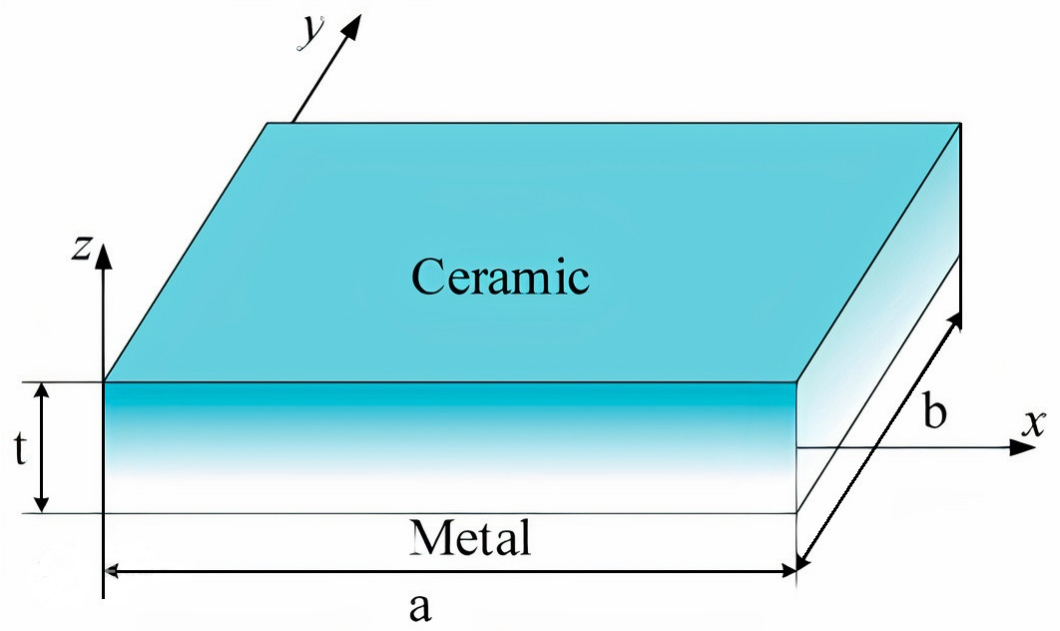

Fig. 1.1 The FG plate model [1]

1.5 Purpose and Necessity of Research Fulfilment

Many structures in the aerospace and mechanical industry are exposed to extensive thermal load and large displacements. Because of it, sometimes instability phenomena like thermal post-buckling occur. Some shuttle components, such as its body and combustion chamber, tolerate extremely high thermomechanical loads without defeat above the buckling domain and go to the post-buckling area. Thus it is necessary to use materials that can show acceptable behavior to thermal loads.

FGMs, known as a new class of heterogeneous composite materials, can be the same thing mentioned. Their volume fraction is continuously distributed in the chosen direction. FGMs have reduced the intensity of stresses, especially thermal stresses, and have the ability to withstand extreme temperature gradients. Since it has high strength and high temperature resistance, it is also used as the coating of the space shuttle. The temperature varies simultaneously as the shuttle is exposed to thermal stress while passing through the atmosphere layer. Hence, it is better to regard the accurate temperature distribution in the design and analysis of the functionally graded (FG) plate. Also, temperature-dependent properties should be considered for them to get more accurate results.

Since at high temperatures, the plates start buckling, thus, it is essential to use a

trustworthy method for studying the stability and thermal post-buckling of FG plates. So designers should investigate the thermal post-buckling of structures by precise computation. Until now, the thermal post-buckling analysis of FG plates is not done based on CUF. Therefore, the main purpose of this study is the thermal buckling and post-buckling analysis of rectangular FG plates with temperature-dependent properties using CUF.

1.6 Literature review

In this section background of buckling, thermal buckling, post-buckling, and FG plate is widely investigated:
In 1991, Gary and Mei scrutinized the thermal post-buckling behavior of composite plates by utilizing FEM. They acquired the plate's governing equations based on von Karman relations employing the principle of virtual work and compared FEM results with the available analytical methods. Furthermore, they saw the effect of the temperature dependency of materials on the plate's buckling response [14]. In 1991, Chang and Liu analyzed the thermal buckling of an antisymmetric angle-ply multilayer rectangular plate. They modeled the plate by shear and normal transverse strains using a high-order deformation theory, as well as fully simply supported (SSSS) conditions and uniform heat loads. By reducing the order of this theory, they were able to compare their work with the FSDT and HSDT, and observed that there was a great difference between the two theories and their theory. The reason for this difference was to consider the effect of normal transverse strain in the thermal buckling analysis of this plate [15]. In 1991, Chen et al. considered both uniform and non-uniform temperature distribution to analyze the thermal buckling and post-buckling of multilayer composite plates and solved it using FEM. They considered the properties of the plate to be temperature dependent. Utilizing the principle of minimum potential energy, they extracted the non-linear stiffness matrix and the geometric stiffness matrix. They used one of the iterative methods to obtain the thermal post-buckling path and concluded that the properties' dependency on the temperature has a significant effect on the post-buckling behavior of the plate. They also concluded that the critical temperature depends on the angle of the layers, aspect ratio, and type of temperature distribution [16, 17]. In 1993, Thornton studied the role of temperature distribution across the thickness and also the material's

thermal properties on the plate's post-buckling. He got the thermal buckling load by experimental and analytical methods [18]. In 1994, Prabhu and Danaraj considered laminate plates with different boundary conditions and analyzed thermal buckling using the finite element method based on the Riessner-Mindlin deformation theory. They investigated the effect of stress distribution on the critical temperature and also included the shear correction factor in their analysis [19]. Shen, in 1997, combined the perturbation approach and Galerkin method to examine the thermal post-buckling of an imperfect geometrically laminate plate surrounded by uniform and nonuniform temperature distribution by using HSDT. He also concluded that the plate's thermal buckling load is influenced by the transverse shear strain, direction of the fiber, aspect ratio, and initial defect [20]. In 2001, Singha et al. examined the path of post-buckling for composite plates imposed by uniform temperatures using FEM. They reached the critical thermal buckling load by increasing the temperature through the thickness of the plate; in other words, they employed the refined Newton-Raphson approach to get the temperature-deflection graph [21]. In 2002, Javaheri and Eslami extracted the equilibrium and stability equations for FG rectangular plates based on the CPT and HSDT in two papers and solved them by an analytical solution method. They applied heat in four ways, uniformly, linearly, and nonlinearly along with the plate thickness and linearly along with the plate length, and concluded that the critical temperature value obtained according to HSDT was less than the critical temperature value obtained from CPT. They also found that by increasing the aspect ratio of the width to the length of the plate and increasing the width-to-thickness ratio of the plate, the critical temperature increases and decreases, respectively. Another result of these two studies was that the critical temperature resulting from the application of heat load along with the length of the plate was higher than the critical temperature obtained from the application of linear heat load along with the thickness of the plate [22, 23]. In 2004, Liew et al. investigated the FG laminate plates' thermal post-buckling according to FSDT. They used the minimization of strain energy principle to compute the critical thermal buckling load of the FG plate whose materials were dependent on temperature [24]. In 2004, the thermal buckling analysis of thick rectangular FG plates with SSSS boundary conditions was investigated by Lanhe, assuming the FSDT. He used exponential law in order to model the gradual change of materials along with the thickness of this plate and concluded that by increasing the amount of exponential power in this plate, the critical buckling temperature decreases. He also found that transverse shear deformation

has a significant effect on the critical buckling temperature of FG plates, especially thick plates [25]. Eslami and Shariat, in 2006 and 2007, scrutinized the thick FG plates' buckling behavior under thermomechanical loads and extracted the governing equations of the plate utilizing third-order shear deformation theory (TSDT). They deemed the uniform and nonlinear temperature distribution in the thickness direction. They inferred that the critical thermal load for the thick plate, assuming CPT, is larger than that of FSDT, and as well as the critical temperature obtained from FSDT is higher than that of TSDT. They suggested employing the TSDT to obtain a more precise thermal buckling load. They also discovered the thick plate started to buckle at a very high temperature when nonlinear temperature distribution across the thickness is used in comparison with utilizing uniform distribution [26–28]. In 2007, Kordkheili and Naqdabadi, by utilizing the Lagrangian description, derived a nonlinear governing equation of FG shells and plates. They acquired temperature distribution through the thickness by solving the nonlinear equation of heat transfer employing Raileigh-Ritz technique. They validated the outcomes of their work with similar studies that were solved analytically, contemplating large deflections [29]. In 2009, Khalili et al. investigated the buckling control of smart FG plates utilizing piezoelectric sensor/actuator patches. They considered an FG rectangular plate with SSSS boundary condition that has piezoelectric patches connected to the bottom or top surfaces in order to operate as actuators. They extracted the governing motion equations using CLT under a constant electric charge. The Fourier series approach is used to solve the equation of motion, and the impact of feedback gain on the buckling load is analyzed by them [30]. In 2010, Sobhy and Zenkour investigated the thermal buckling behavior of different kinds of sandwich FG plates utilizing sinusoidal shear deformation theory. The bottom and upper layers of the sandwich plate are created from FGM and its core is ceramic. Their upshots indicated that the thermal buckling load received from the theory is smaller than that of getting from CPT. The FG sandwich plate's critical temperature is inferior to the critical temperature of the ceramic-rich plate [31]. In 2012, Mohammadi and Khalili analyzed the free vibration of FG sandwich plates in various thermal loading. They supposed that the core properties are not only temperature dependent but also vary gradually in the direction of thickness based on a power-law distribution according to volume fractions of the plate. They used a new technique to reduce motion equations from twenty-three to eleven and then could solve them. Their new solution had been consisted of separating six of the unknowns in the face sheets' displacements utilizing the

compatibility equations, then separating the extra six Lagrange multipliers employing the face sheets' equations. Consequently, they replaced the separated unknowns into the core's eleven equations. They found good agreement between their work's results and the outcomes acquired by similar references for SSSS sandwich plates with FG face sheets [32]. In the years 2011 to 2014, Fazzolari and Carrera proposed advanced Ritz, Galerkin, and generalized Galerkin methods based on quasi-three-dimensional order models to analyze the thermal buckling of composite plates and multilayer sandwich plates based on the principle of virtual displacement. They concluded that when it is not possible to ignore the three-dimensional effects in the thermal buckling analysis of sandwich structures, it is necessary to use high-order improved theories that incorporate the effect of vertical transverse deformation. An important advantage of these theories, which include the ESL, ZZ, and LW models, is that the accuracy of the results can be raised by extending the number of kinematic variables. By increasing and decreasing the order of the improved theories, thick and thin plates, respectively, can be well modeled and analyzed [33–40]. In 2015, Bouguenina et al. investigated the thermal buckling behavior of a linearly variable-thickness FG plate. They first extracted the equations of thermal stability under uniform heating in the direction of thickness and analyzed them by the finite difference method. Then they compared the results of the numerical method with the results of an analytical solution as well as the results of similar articles and showed the accuracy of their solution method. Their parametric studies proved that the thermal resistance of the FG plate increases with increasing rigidity and thickness [41]. In 2016, Lee et al. investigated the thermal buckling behavior of the FG plate according to the neutral plane. They selected the neutral plane, not the plate's middle surface, as the reference. The plate's materials depend not only on the thickness direction but also on temperature. The neutral plane location is got regarding temperature variations. They operated FSDT and 1D heat transfer equations in the calculations. They concluded that while the elastic modulus of the metal is smaller than that of ceramic, the neutral plane locomotes away from the plate's middle surface and is located in the ceramic part [42]. In 2017, Yu et al. investigated an FG rectangular plate's thermo-mechanical buckling using a unique numerical approach. They examined the buckling response using FSDT and isometric analysis without assuming the shear-locking effects. They employed the exponential law for the distribution of the FG plate and inferred that by increasing the volume fraction index from 0 to 1, the plate goes toward an instability regime. They likewise saw the plate with fully clamped

(CCCC) boundary conditions is more stable than the plate with SSSS boundary conditions [43]. In 2018, Megueni and Daikh studied the thermal buckling response of a sandwich FG plate using HSDT. The plate was under several kinds of thermal load across the thickness. They offered a new solution for the nonlinear thermal distribution and found that the critical temperature resulting from the nonlinear temperature distribution is higher and more accurate than the two others [44]. In 2018, Trabelsi et al. analyzed the thermal post-buckling of FGM structures utilizing FEM. They proposed geometrically nonlinearity according to a modified FSDT. They employed large displacement based on Green-Lagrange strains in their study and used a parabolic shape function to modify the shear strains in the structure. They proved that their method has high accuracy and effectiveness for getting results [5]. In 2019, Wu et al. examined the post-buckling path and large deflection of an isotropic rectangular plate utilizing CUF. To solve the plate's nonlinear governing equations, they employed Newton-Raphson and could get nodal displacement versus load [45]. In 2021, Sadgui and Tati used FEM based on a rectangular element with hypothetical natural shear strains to analyze mechanical buckling and free vibration of FG plates. They utilized a new HSDT with only five unknowns and supposed no transverse shear stress at the up and down of the plate, so it was not necessary to use a shear correction coefficient. They proved the accuracy of their formula by comparing it with the results of other authorities [46]. In the middle of 2021, Tahir et al. analyzed the hygro-thermal behavior of wave propagation in porous FG sandwich plates. Their sandwich plates were divided into two types, each of which had three layers. The top and bottom layers of both included porous FGM graded according to a power law. But one had a rich metal core, while another had a rich ceramic one. Their study was accomplished HSDT with an uncomplicated four-unknown. The governing equations of the problem were derived from Hamilton's principle. Their results were acquired by an eigenvalue problem [47]. In 2021, the buckling behavior of FG plates with SSSS boundary conditions was examined by Ahmed et al. using HSDT. The proposed formula does not use a shear correction factor but modifies the transverse stress. In their work, the properties of the material are presumed to vary based on the power law through the thickness direction. They investigated the effects of the aspect ratio and volume fraction index of the plate on critical buckling load [48]. In 2021, Zaitoun et al. studied the buckling behavior of an FG sandwich plate considering heat-humidity conditions. An exact solution was created using HSDT with just four unknowns. Their sandwich plate had three layers. They offered three

different types of FG sandwich plates in terms of arrangement and layer composition. Motion equations were derived based on the Hamilton principle. Then Navier's analytical solution was used to get the buckling temperature for an FG sandwich plate with SSSS boundary conditions resting on a viscoelastic foundation [49]. In 2021, Kadapa, in order to obtain the load-deflection path of nonlinear equilibrium of structural problems, used the arc-length method in the framework of FEM. In his modified technique, the predictor is calculated by extrapolating the results from two earlier converged load steps. The suggested extrapolated predictor provides a way to follow forward motion along the path of equilibrium without employing any complex methods usually utilized for explicit tracking. He proved the accuracy of his suggested method by solving the nonlinear governing equations of some structural examples such as trusses, columns, and shells. [50]. In 2021, Farrokh et al. analyzed the thermal and mechanical buckling behavior of the rectangular FG plate. They use three types of temperature distribution for the thermal case: uniform, linear, and nonlinear. They also employed CUF for modeling and analyzing the plate. In their study, boundary conditions of convection heat transfer had a profound influence in acquiring critical thermal buckling load [51]. In early 2022, Rachid et al. investigated free vibration and bending of FG double-curved shells under mechanical sinusoidal and uniform loads. The purpose of their paper was to develop a new formulation of 2D and quasi-3D HSDT with setting the influencing of transverse shear. Numerical results are reported for different geometries, such as plates and spherical shells employing a five-unknown displacement field. Their suggested theory confirms proper in the study of FG double-curved shells [52]. In 2022, Khosravani et al. investigated the mechanical and thermal properties of the constituent materials of some kinds of composites using a multiscale method based on CUF. They concluded that the strange behavior of some composites under thermal load can be justified from a microscopic point of view and is attributed to factors such as the difference value in modulus of elasticity, coefficient of thermal expansion and thermal conductivity of each component in a composite [53, 54]. In 2022, Farrokh et al. optimized the distribution of materials for FG plates in order to maximize the critical buckling temperature subjected to thermal load. They employed three models of distribution to minimize the materials utilized in the FG plate. The outcomes of their work show that by increasing the degrees of freedom corresponding to the material distribution, the FG plate's thermal buckling load is raised. They also discovered that the optimum distributions acquired did not rely

on the FG plate's boundary conditions and geometry [55]. In 2023, Kumar et al., using FEM based on modified TSDT in conjunction with a neural network, estimated the buckling load of a carbon nanotube (CNT) reinforced hybrid FG plate. They assumed a zero transverse shear deformation for their results. Employing the random value in the material's properties as an input parameter and considering the critical buckling load as an output parameter, a problem based on the machine learning method is defined by them to predict the buckling behavior of the CNT reinforced hybrid FG plates. They developed a C^0 FEM code in MATLAB software, validated the modified TSDT with previous similar works, and discovered their method is suitable for obtaining accurate results [56]. In 2023, Tavakoli et al. investigated the Gaussian random fields in the mechanical properties of the composite plate and its effects on the buckling load. In their work, the random fields were decayed by the KarhunenLoève approach and strains were determined based on FSDT. They extracted motion equations employing the Euler–Lagrange formula. They analyzed the effect of spatially varying random properties on the plate's critical buckling load and corresponding mode shapes for the first time. Their results demonstrated that different shear deformation theories could seriously affect the stability of thick plates when compressive loads are applied [57]. Chen et al., in 2023, conducted a study investigating the compressive and thermal post-buckling responses of porous sandwich plates. In their study, the graphene platelets reinforced composite core was made of several layers with different values of graphene porosity to receive an FG model. They extracted the governing equations for the thermal post-buckling of porous sandwich plates based on Reddy's TSDT and by considering the von Kármán nonlinear strain–displacement. They acquired results by analyzing some numerical studies and compared their outcomes with an equivalent isotropic model. Their results show the equivalent isotropic model is not proper for thermal buckling and post-buckling analysis of porous plates [58]. In 2023, Wang et al. scrutinized the post-buckling paths of the composite laminated plates reinforced by fiber under the thermal load. They obtained the governing equations based on the nonlinear Von Karman relation and using the TSDT and Hamilton's principle. The consequences of their study revealed that the limit points through unstable paths have a direct relationship with the negative eigenvalues in the initial position in the post-buckling region. They found that, in the flat plate, buckling deformation remains the same under varying perturbation loads as long as the perturbation load is small. Also, in the case of a plate with low defects, the buckling deformation is like that of

an isotropic plate. But if the defect of the plate is more significant, the buckling deformation would be high [59]. Therefore, it is necessary to use a reliable method for checking the stability of the FG plate. CUF, in the framework of FEM, is an appropriate method for thermal buckling and post-buckling analysis of the plate.

1.7 Thesis Outline

This thesis consists of 6 chapters; each chapter's objectives and outline are as follows:

1. The first chapter has presented the overview, problem definition, purpose and literature review of the thesis.

2. The second chapter has defined FG plates with temperature-dependent properties and their governing equations. It has also explained the procedure for obtaining the temperature distribution within the thickness of the FG plate by applying FEM over the heat transfer equation.

3. The third chapter has described structural theories and Carrera Unified Formulation. In addition, this chapter has expressed the fundamental concept of a continuous body, like displacement, strain, and stress. Also, thermal stresses and strains stemming from the imposed heat are calculated to obtain thermal load in this chapter.

4. The fourth chapter has derived the Nonlinear equilibrium equation of the FG plate under thermal loading. It has also explained the solution procedure of the governing equation by an increment-iterative method in the thermal post-buckling analysis. Furthermore, the linear buckling analysis in order to get critical temperature has been explained.

5. The fifth chapter includes the results and discussion of several numerical examples for analyzing thermal buckling and post-buckling of the FG plate with and without considering temperature-dependent properties.

6. The sixth chapter presents the conclusion of the present study, suggests similar future works and shows the extracted journal papers from this thesis.

Chapter 2

FG plates with temperature-dependent properties and temperature distribution

2.1 Introduction

FGMs for the first time introduced in 1984 by Japanese researchers in a space project. The gradual and continuous change of properties within thickness gives it a preference rather than laminates and other composites due to their mechanical and thermal behavior. Temperature also changes within the thickness of plates for various reasons, so it is essential to calculate the profile of temperature with an accurate approach. Furthermore, investigating temperature-dependent properties of FG plates and modeling their equations to the problem properly is of great significance.

2.2 FG plates

FGMs create a harmony of thermal and mechanical properties because it is built of a hybrid of ceramic and metal. One side of these plates is produced purely from ceramics and the other side of them is entirely made of metal, and the distance between sides is a combination of both of them. Metal properties gradually decrease

from the rich metal face to the fully ceramic face and contrariwise. A schematic of an FG plate is shown in Fig. 2.1

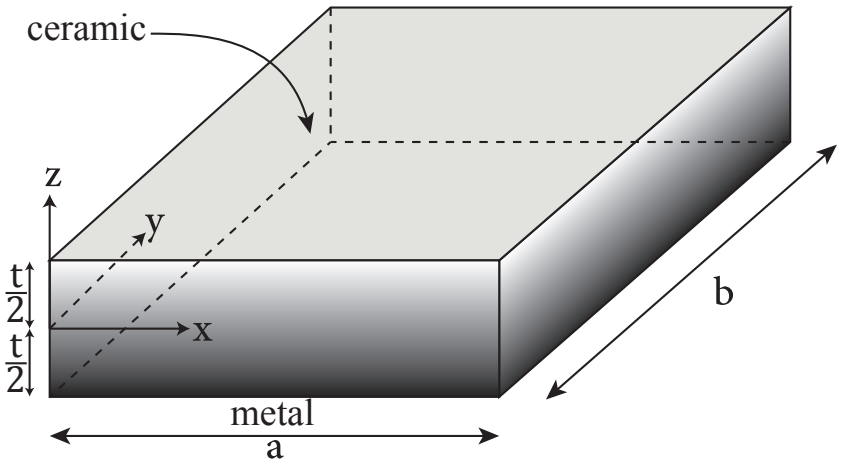

Fig. 2.1 The FG plate schematic.

2.3 FG plates with temperature-dependent properties

Different material gradation laws have been proposed by scientists and researchers for FGM. In this research, the properties of the material based on volume fractions have been assumed not only to vary through the plate thickness direction but also to vary with temperature. It should be mentioned, different material gradation laws such as sigmoid or exponential low have been proposed for FGM in the literature. In this thesis, the power-gradation law has been adopted. According to it, the relation described properties of temperature-dependent FG plate and the volume fraction of ceramic v_c and metal v_m are as follows [60]:

$$v_c = (\frac{z}{t} + \frac{1}{2})^n \tag{2.1}$$

$$v_m = 1 - v_c \tag{2.2}$$

$$P(T,z) = (P_c(T) - P_m(T))\, v_c + P_m(T) \tag{2.3}$$

$$P_i = P_0(P_{-1}T^{-1} + 1 + P_1T + P_2T^2 + P_3T^3) \tag{2.4}$$

In Eq. (2.1), n is power index that controls the volume fractions, z is thickness coordinate, t is thickness of the considered FG plate in Fig. 2.1. In Eq. (2.3), T is temperature distribution through the thickness and P denotes material property such as elasticity modulus E, thermal conductivity coefficient k, thermal expansion coefficient α and Poisson ratio ν. In this thesis, subscripts c and m refer to ceramic and metal constituents, respectively. In Eq. (2.4), i can be c or m. Also, P_0 , P_{-1} , P_1 , P_2 , P_3 are such constants that are given in Table 2.1. Since the above equations are temperature dependent, temperature distribution along with the plate thickness must be calculated. It must be noted that in this work, in a section, all properties, even thermal conductivity coefficient, have been considered temperature-dependent. While in the other section, it has considered the properties of FGM to be independent of temperature. Thus, Table 2.2 is shown here to present the temperature-independent properties of some materials.

Table 2.1 Temperature-dependent coefficients of materials properties E(Pa), $\alpha(1/K)$, ν and $k(W/mK)$ in FGM [7] , [4]

Material	Properties	P_0	P_{-1}	P_1	P_2	P_3
Ti-6Al-4V	E_m	122.56e+9	0	-4.586e-4	0	0
	α_m	7.5788e-6	0	6.638e-4	-3.147e-6	0
	ν_m	0.29	0	0	0	0
	k_m	1.0000	0	1.704e-2	0	0
ZrO_2	E_c	244.27e+9	0	-1.371e-3	1.214e-6	-3.681e-10
	α_c	12.766e-6	0	-1.491e-3	1.006e-5	-6.778e-11
	ν_c	0.29	0	0	0	0
	k_c	1.7000	0	1.276e-4	6.648e-8	0
Ni	E_m	223.95e+9	0	-2.794e-4	3.998e-9	0
	α_m	9.9209e-6	0	8.705e-4	0	0
	ν_m	0.31	0	0	0	0
	k_m	187.66	0	-4.614e-4	6.670e-7	-1.523e-10
Si_3N_4	E_c	348.43e+9	0	-3.070e-4	2.160e-7	-8.946e-11
	α_c	5.8723e-6	0	9.095e-4	0	0
	ν_c	0.24	0	0	0	0
	k_c	13.723	0	-1.032e-3	5.466e-7	-7.876e-11
SUS304	E_m	201.04e+9	0	3.079e-4	-6.534e-7	0
	α_m	12.330e-6	0	8.086e-4	0	0
	ν_m	0.31	0	0	0	0
	k_m	15.379	0	-1.264e-3	2.092e-6	-7.22e-10

Table 2.2 Temperature-independent properties of the Nickel and Alumina [5]

Properties	Ni	Al_2O_3
E (Pa)	199.5e+9	393e+9
$\alpha(1/K)$	13.3e-6	8.8e-6
$k(W/mK)$	90.7	30.1
ν	0.30	0.25

2.4 Calculation of temperature distribution by FEM

In some articles, either the assumed distribution is used to calculate the temperature distribution along with the thickness of an FG plate, or the analytical solution of the Fourier law by the power series method with a limited number of terms. However, in this study, the temperature distribution in the thickness direction is obtained by solving the heat conduction equation with an iterative method using FEM, which makes it possible to increase the number of partitions in the thickness direction in order to get a more accurate and realistic temperature distribution. The description of this method is as follows:
In the beginning, a brief definition of conduction and convection heat transfer is given. Convection is a kind of heat transfer that results from the movement of fluid particles, such as gases and liquids. If this type of heat transfer will be occurred by the fluid located to the structure's adjacency, herein named convection boundary condition. Conduction is another kind of heat transfer, in which heat conducts by the ingredient of material. In other words, at first, a part of the material will be heated and the molecules of the mentioned part will be moved further. Then, will collide with their neighbor molecules and move them. This procedure will continue in the whole material so much so that it becomes completely heated. Now, according to these definitions, the process of achieving the temperature distribution is described in an FG plate with surrounding fluid on both sides of it. Temperature distribution through the thickness can be obtained by solving the 1D steady-state thermal conductivity equation.

$$\frac{\partial}{\partial z}(k(T,z)\frac{\partial T}{\partial z}) = 0 \tag{2.5}$$

under the following convection boundary conditions [51]:

$$\begin{aligned} k_m \tfrac{dT}{dz}\big|_{-t/2} &= h_m(T_m - T_m^e) \\ -k_c \tfrac{dT}{dz}\big|_{t/2} &= h_c(T_c - T_c^e) \end{aligned} \tag{2.6}$$

In Eq. (2.5), k and z represent thermal conductivity coefficient and one of the coordinate's components in direction of thickness. In Eq. (2.6), k_m and k_c indicate metal and ceramic thermal conductivity coefficient and h_m and h_c are convection heat transfer coefficients for the surrounding fluids near the metal-rich and ceramic-rich faces of the plate, respectively. Also T_m and T_c show metal and ceramic temperature

while T_m^e and T_c^e stand for the temperatures of the surrounding fluids near the metal-rich and ceramic-rich faces, respectively. If h_m and h_c lead to infinity, it can be shown both of them by h and this causes the temperature adjacent to the metal to be equal to the temperature of the metal surface and the temperature adjacent to the ceramic to be equal to the temperature of the ceramic surface. Due to the fact that k is the function of both temperature and position simultaneously, it has a complicated analytical solution. Hence, a numerical method like FEM can be helpful to obtain temperature distribution with governing boundary conditions.

2.4.1 Heat transfer formulating by FEM

If heat is transferred in a continuous environment, it is possible to convert this continuous environment to a discrete environment using FEM and use its relations to calculate the temperature distribution. In FEM, a domain is divided into several elements that have common nodes with themselves. Then by using the governing equation, element quantities will be calculated. By assembling them, the governing equation of the whole domain will be solved. It is worth mentioning that the variable field interpolation in each element will be performed by the shape function of the target element:

$$\begin{aligned} T &= \mathbf{N}\mathbf{T}^e \\ \mathbf{N} &= \{N_1, N_2, ...N_q\} \\ \mathbf{T}^e &= \{T_1, T_2, ...T_q\}^T \end{aligned} \tag{2.7}$$

In which $\mathbf{N}$ and $\mathbf{T^e}$, respectively are shape function and nodal temperature vectors of an element with q nodes. By assuming $\mathbf{L} = \frac{\partial}{\partial z}$ and applying the Galerkin method in Eq. (2.5), Eq. (2.8) will be obtained.

$$\int_{\Omega^e} \mathbf{N}^T (\mathbf{L}(k\mathbf{L}\mathbf{N}\mathbf{T}^e)) dv = 0 \tag{2.8}$$

Considering $\mathrm{B} = \mathbf{L}\mathrm{N}$ and applying convection boundary conditions, Eq. (2.9) will be obtained.

$$(\mathbf{K}_c^e + \mathbf{K}_h^e)\mathbf{T}^e = \mathbf{R}_h^e \tag{2.9}$$

In which:

$$\begin{aligned}\mathbf{K}_c^e &= \int_{\Omega^e} k\mathrm{B}^T\mathrm{B}dv \\ \mathbf{K}_h^e &= \int_{s_1} h\mathbf{N}^T\mathbf{N}ds \\ \mathbf{R}_h^e &= \int_{s_2} h\mathbf{T^e}\mathbf{N}^T ds\end{aligned} \tag{2.10}$$

In Eq. (2.10), the subscripts c and h are related to conduction and convection heat transfer, respectively. Also, $\mathbf{K}_c^e$ and $\mathbf{K}_h^e$ are the element matrices resulted from conduction and convection heat transfer respectively, and also $\mathbf{R}_h^e$ is the element vector resulted from temperature distribution and convection heat transfer. For calculating temperature distribution in an FG plate, in addition to knowing the thermal conductivity coefficient of the FG plate, it must be clear convection coefficient of the environment near metal and ceramic separately. After calculation of the element quantities, they will be assembled in order for the heat transfer equation of the whole domain will be obtained.

$$(\mathbf{K}_c+\mathbf{K}_h)\mathbf{T} =\mathbf{R}_h \tag{2.11}$$

If the convection coefficient tends to infinity for both metal and ceramic, only by knowing the conduction heat transfer coefficients and temperature of the metal and ceramic parts, the temperature distribution along with the thickness of the plate will be extracted by using Eq. (2.11). If the aim is to obtain a temperature distribution without considering temperature-dependent properties, Eq. (2.11) could be solved directly, but since the purpose is achieving temperature distribution supposing dependency of properties to temperature, it is needed to use iterative methods to solve it. Hereby, the temperature of all nodes ($\mathbf{T}$) within the thickness of the plate will be reached. Since in this study, the temperature of the metal part is assumed to be constant and the temperature of the ceramic part is variable, through the nodal temperatures obtained along the direction of thickness, the temperature distribution along with the thickness of the plate can be achieved and denoted by $T(z)$ which is a function of the ceramic's temperature. For more clarity, the temperature profile through the thickness of the FG plate with a combination of Nickel/Silicon Nitride (Ni/Si_3N_4) with assuming $0\,K$ for the metal surface and $300\,K$ for the ceramic surface for different volume fraction indexes is shown in Fig. 2.2. It should be noted the figure has been drawn when thermal conductivity coefficients of metal and ceramic are dependent on temperature.

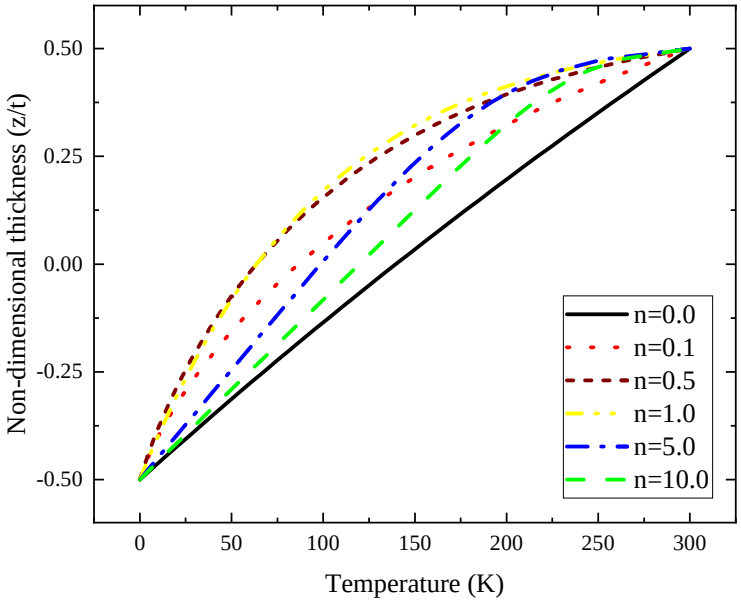

Fig. 2.2 Temperature distribution through the thickness of the FG plate.

Fig. 2.2 illustrates the effects of volume fraction on temperature distribution along the thickness. It is clear from the figure that the linear line related to zero power demonstrates a special kind of FG plate that is the same isotropic plate (pure ceramic). Curved lines show the temperature distribution of different compositions of metal and ceramic.

Chapter 3

Structural Theories and Carrera Unified Formulation

3.1 Classification of plate theories

The theories represented for beams and plates are listed below:

3.1.1 Classical plate theory

This theory assumes that the normal coordinate upon the reference surface will remain perpendicular after deformation, and no warping will occur. It means that transverse shear strain, like normal strain within thickness, is imperceptible.

3.1.2 First-order shear deformation theory

Unlike the previous theory, it contains the transverse shear strain. In other words, each plane that is flat and vertical to mid-plane remains flat but not vertical after deformation. In this theory, shear strains within thickness are considered constant. While in reality, shear stresses vary in thickness and behave parabolically. This difference between real stress and the constant stress considered in FSDT will be roughly resolved by the shear correction coefficient.

3.1.3 Higher-order shear deformation theory

As calculating shear correction coefficient is not simple for many geometries, the modified FSDTs are introduced as higher-order theories. These theories do not require a shear correction coefficient. But the complexity of equations and huge computing cost are considered as deficiencies of these theories.

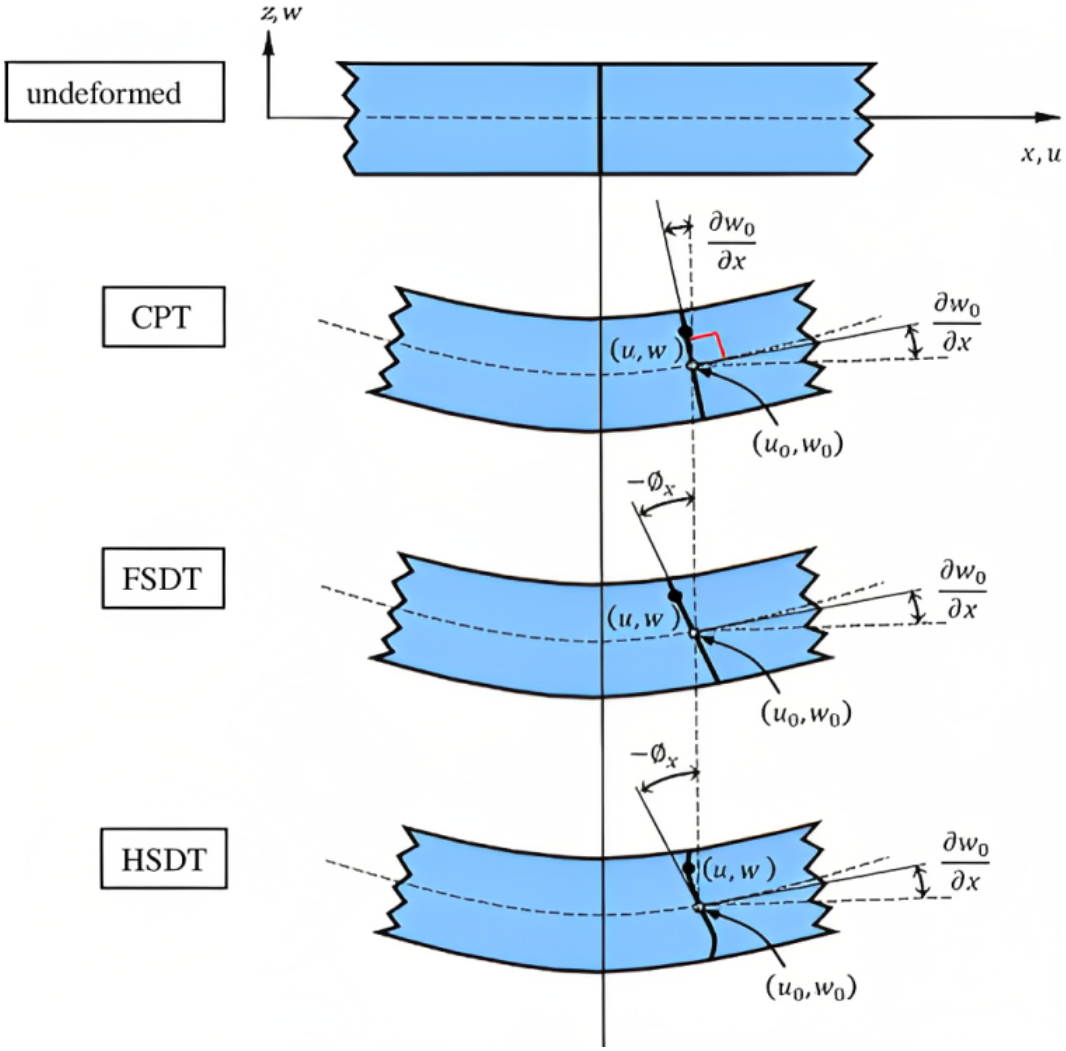

Fig. 3.1 Theories' differences [2]

Figure 3.1 as a $x-z$ cross-section of a plate illustrates the differences between these classifications for better comprehension. In CPT, transverse normal, after deformation, remains perpendicular and straight to the mid-plane. Whereas in FSDT, after deformation, transverse normal again remains straight but no longer

perpendicular to the midplane. It has a deviation in angle and has a linear shape. In HSDT, transverse normal has a curved shape which depicts the higher order of shear deformation.

3.2 Fundamental concept of a continuous body

In Fig. 3.2, a continuous deformable body is demonstrated in a Cartesian coordinate system that is under mechanical loads and boundary conditions.

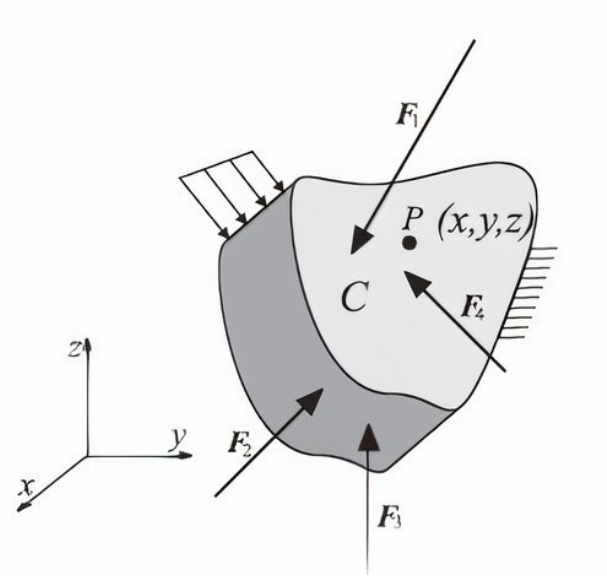

Fig. 3.2 A body under the mechanical loads and boundary conditions

3.2.1 Displacement vector

The displacement of an element is defined as a vector below:

$$\mathbf{u} = [u_x, u_y, u_z]^T \tag{3.1}$$

where $\mathbf{u}$ denotes the displacement vector and u_x, u_y, u_z are the displacement components in three principal directions.

3.2.2 Strain Vector

The strain vector for an element in the Cartesian coordinate system is defined as:

$$\varepsilon = [\varepsilon_{xx}, \varepsilon_{yy}, \varepsilon_{zz}, \varepsilon_{xz}, \varepsilon_{yz}, \varepsilon_{xy}]^{\mathrm{T}} \tag{3.2}$$

where ε is the strain vector, $\varepsilon_{xx}, \varepsilon_{yy}, \varepsilon_{zz}$ are principal strains and $\varepsilon_{xz}, \varepsilon_{yz}, \varepsilon_{xy}$ are shear strains. In the large deformations and Lagrangian description, the Green-Lagrange strain vector have both linear and nonlinear parts:

$$\varepsilon = \varepsilon_l + \varepsilon_{nl} \tag{3.3}$$

where the strain vector is related to the displacement vector by linear and nonlinear operators as below:

$$\varepsilon = (\mathbf{b}_l + \mathbf{b}_{nl})\,\mathbf{u} \tag{3.4}$$

$$\mathbf{b}_l = \begin{bmatrix} \partial_x & 0 & 0 \\ 0 & \partial_y & 0 \\ 0 & 0 & \partial_z \\ \partial_z & 0 & \partial_x \\ 0 & \partial_z & \partial_y \\ \partial_y & \partial_x & 0 \end{bmatrix} \tag{3.5}$$

$$\mathbf{b}_{nl} = \begin{bmatrix} \frac{1}{2}(\partial_x)^2 & \frac{1}{2}(\partial_x)^2 & \frac{1}{2}(\partial_x)^2 \\ \frac{1}{2}(\partial_y)^2 & \frac{1}{2}(\partial_y)^2 & \frac{1}{2}(\partial_y)^2 \\ \frac{1}{2}(\partial_z)^2 & \frac{1}{2}(\partial_z)^2 & \frac{1}{2}(\partial_z)^2 \\ \partial_x\partial_z & \partial_x\partial_z & \partial_x\partial_z \\ \partial_y\partial_z & \partial_y\partial_z & \partial_y\partial_z \\ \partial_x\partial_y & \partial_x\partial_y & \partial_x\partial_y \end{bmatrix} \tag{3.6}$$

in which $\partial_x = \frac{\partial(.)}{\partial x}$, $\partial_y = \frac{\partial(.)}{\partial y}$ and $\partial_z = \frac{\partial(.)}{\partial z}$.

3.2.3 Thermal Strain

Thermal strain is created due to changes in temperatures. In other words, a structure is expanded and deformed because of the temperature increment.

Thermal strain of 1D structure

Change in length of a 1D structure results from heat is calculated by equation (3.7):

$$\Delta L = L_0 \alpha \Delta T \tag{3.7}$$

where ΔL represents the length's change, L_0 is the initial length and ΔT is the temperature increment. By dividing ΔL over L_0, the thermal strain of a bar can be computed by equation (3.8):

$$\varepsilon_T = \frac{\Delta L}{L_0} = \alpha \Delta T \tag{3.8}$$

Thermal strain of 3D structure

By generalizing equation (3.8), the thermal strain ε_T for a 3D structure is obtained by equation (3.9):

$$\begin{aligned} &\varepsilon_T = \alpha \Delta T \\ &\alpha = \{\alpha_x, \alpha_y, \alpha_z, 0, 0, 0\}^{\mathrm{T}} \end{aligned} \tag{3.9}$$

In which α is the vector of thermal expansion coefficient and α_x, α_y and α_z are coefficients of thermal expansion in direction of x, y and z, respectively. Since they are not constant, all of them are modeled according to relation (2.3).

3.2.4 Stress vector

In this research, σ shows vector of stress:

$$\sigma = [\sigma_{xx}, \sigma_{yy}, \sigma_{zz}, \sigma_{xz}, \sigma_{yz}, \sigma_{xy}]^{\mathrm{T}} \tag{3.10}$$

It is in relation with mechanical strain ε and thermal strain vector ε_T as follows:

$$\sigma = \mathbf{C}(\varepsilon - \varepsilon_T) \tag{3.11}$$

In which **C** is the constitutive matrix (connector matrix between stress and strain):

$$\mathbf{C} = \begin{bmatrix} c_{11} & c_{12} & c_{13} & 0 & 0 & 0 \\ c_{12} & c_{22} & c_{23} & 0 & 0 & 0 \\ c_{13} & c_{23} & c_{33} & 0 & 0 & 0 \\ 0 & 0 & 0 & c_{44} & 0 & 0 \\ 0 & 0 & 0 & 0 & c_{55} & 0 \\ 0 & 0 & 0 & 0 & 0 & c_{66} \end{bmatrix} \tag{3.12}$$

where c_{ij} for an FG plate with temperature-dependent properties are functions of elasticity modulus and Poisson ratio explicitly and temperature implicitly as follows [61]:

$$\begin{aligned} c_{11} = c_{22} = c_{33} &= \frac{E(T(z),z)(1-\nu(T(z),z))}{(1+\nu(T(z),z))(1-2\nu(T(z),z))} \\ c_{44} = c_{55} = c_{66} &= \frac{E(T(z),z)}{2(1+\nu(T(z),z))} \\ c_{12} = c_{13} = c_{23} &= \frac{E(T(z),z)\nu(T(z),z)}{(1+\nu(T(z),z))(1-2\nu(T(z),z))} \end{aligned} \tag{3.13}$$

3.3 FEM analysis based on Carrera Unified Formulation

The method of CUF in FEM is similar to the separation of variables in mathematics. Displacement vector is a function of x, y, z separated to shape function N and expansion function F as below [13]:

$$\mathbf{u} = F_\tau N_i \mathbf{u}_{\tau i} \tag{3.14}$$

where $\mathbf{u}_{\tau i} = [u_{x_{\tau i}}, u_{y_{\tau i}}, u_{z_{\tau i}}]^T$ is nodal displacement vector of generalized coordinates, in which subscript $i = 1, 2, \ldots, w$ shows the node number and w stands for the total nodes utilized per element. While in subscript $\tau = 1, 2, \ldots, M$, the summation pattern with the repetitive index τ is supposed, and M indicates the expansion's order.

CUF has three models for separating the displacement vector into shape function and expansion function:

3.3.1 1D model

In this model, according to Fig. 3.3, the shape function is 1D and the expansion function is 2D. This model is applied in beams.

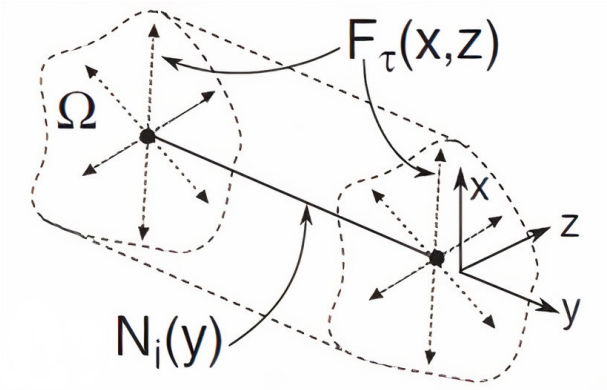

Fig. 3.3 Description of a body with 1D shape function and 2D expansion function

$$\mathbf{u} = F_\tau(x,z) N_i(y) \mathbf{u}_{\tau i} \tag{3.15}$$

3.3.2 2D model

In this model, the shape function is 2D and the expansion function is 1D. It is shown in Fig. 3.4. This model is used for modeling and analyzing plates and shells. In this research, the 2D model is utilized.

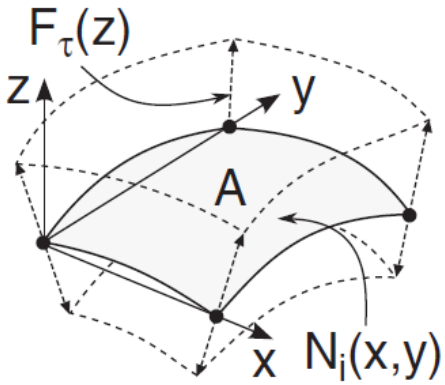

Fig. 3.4 Description of a body with 2D shape function and 1D expansion function

$$\mathbf{u} = F_\tau(z) N_i(x,y) \mathbf{u}_{\tau i} \tag{3.16}$$

3.3.3 3D model

In this model, the shape function is 3D and the expansion function does not exist. This model is the same as classical FEM. It is employed for analyzing 3D bodies as shown in Fig. 3.5.

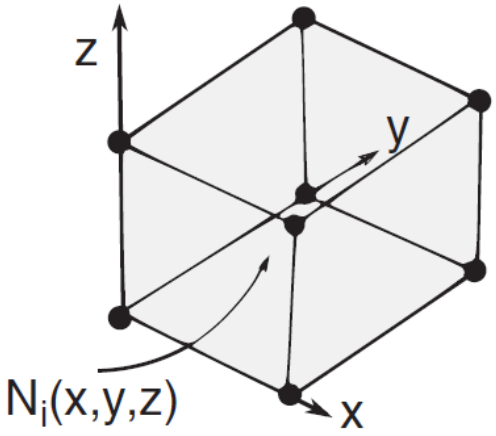

Fig. 3.5 Description of a body with 3D shape function

$$\mathbf{u} = N_i(x,y,z) \mathbf{u}_{\tau i} \tag{3.17}$$

3.3.4 Taylor expansion function

As in this research, the analysis is done on the plate, thus the 2D model has been selected. Therefore, Taylor-like polynomial is used as 1D expansion function that is represented in Eq. (3.18).

$$F_\tau(z) = z^{\tau-1} \tag{3.18}$$

It should be mentioned, in the expansion function, any order can be assumed to model the kinematics of the plate in the thickness direction.

3.3.5 Lagrange shape function

In this study, Lagrange polynomials are used as 2D shape functions of a nine-node standard element. The element is illustrated in Fig. 3.6, and the shape functions are as follows:

$$\begin{aligned}
N_1 &= \frac{1}{4}(\xi^2-\xi)(\eta^2-\eta)\\
N_2 &= \frac{1}{2}(1-\xi^2)(\eta^2-\eta)\\
N_3 &= \frac{1}{4}(\xi^2+\xi)(\eta^2-\eta)\\
N_4 &= \frac{1}{2}(1-\eta^2)(\xi^2+\xi)\\
N_5 &= \frac{1}{4}(\xi^2+\xi)(\eta^2+\eta)\\
N_6 &= \frac{1}{2}(1-\xi^2)(\eta^2+\eta)\\
N_7 &= \frac{1}{4}(\xi^2-\xi)(\eta^2+\eta)\\
N_8 &= \frac{1}{2}(1-\eta^2)(\xi^2-\xi)\\
N_9 &= (1-\xi^2)(1-\eta^2)
\end{aligned} \tag{3.19}$$

where ξ, η are the element's local coordinates and can change between $[-1,1]$. As the geometry considered in this research is the rectangular plate, just the rectangular

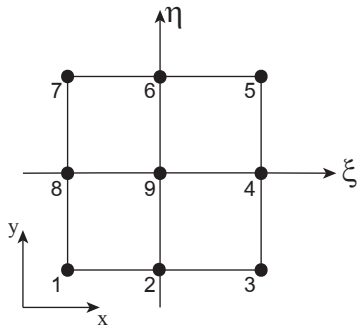

Fig. 3.6 A 2D standard element with nine nodes.

elements are utilized in the FEM's mesh. Thus, the relation between ξ, η with x, y of global coordinates are presented as:

$$\begin{aligned} \xi &= \frac{2(x-x_1)-l_x}{l_x} \\ \eta &= \frac{2(y-y_1)-l_y}{l_y} \end{aligned} \tag{3.20}$$

where x_1, y_1 are coordinates of Node 1 from the element illustrated in Fig. 3.6, and l_x, l_y, respectively, are each element's length and width.

Chapter 4

Nonlinear equilibrium equation of FG plate

4.1 Introduction

This chapter shows how to derive the nonlinear equilibrium equation of FG plate under thermal loading. As mentioned before, the aim of this research is to analyze the thermal post-buckling of the FG plate with temperature-dependent properties. Searching among the previous studies in the field of plates' post-buckling analysis, it was clarified that the assumptions of large deflection in plates must be employed. By doing so and using the virtual work principle, the governing nonlinear equilibrium equations of the FG plate are acquired. In some related papers, a particular kind of these equations are well-known as von Karman. They are such equations with nonlinear partial differential operators so that some real practical problems can be modeled by them. But, finding the analytical solution for them is too complicated and is able to solve a limited range of problems analytically. Therefore it is necessary to derive the matrix form of these equations. Then, they can be solved by numerical methods like FEM based on CUF. In 2019, a paper was published by Wu et al. in which they analyzed large deflection and post-buckling of rectangular isotropic plates based on CUF. They utilized the principle of virtual work to drive equilibrium equations by considering nonlinear terms of strain according to Green-Lagrange strain. In the following of this chapter, in order to model and analyze the thermal post-buckling of the FG plate, a similar technique with some changes is applied for

obtaining nonlinear equilibrium equations under thermal load and also is presented the solution procedure of the thermal buckling and post-buckling of the FG plate.

4.2 Thermoelastic Problems

Thermoelasticity is an expansion of the elasticity theory in which temperature changes, in addition to imposing mechanical forces, cause deformation and strains. Extracting governing equations is extremely complicated by inputting the temperature field in the continuous deformable body analysis. The complication occurs when mechanical and thermal fields are coupled together. In this state, a continuum will experience a temperature variation as a result of deformation and vice versa. Though basically, it is usually feasible to ignore their coupling and consider the deformation and temperature fields separately. But in this study, partially coupled thermoelastic is considered not only to prevent huge complications but also to have accurate results.

4.2.1 Partially Coupled Thermoelastic Problems

Partial coupling in thermoelasticity refers to the situation where thermal effects influence the deformation behavior of a material, but the deformation does not affect the temperature field. In other words, the heat transfer influence on strain and stress fields, while the strain and stress fields do not influence the temperature. In partially coupled thermoelastic problems, the governing equations for both the thermal and mechanical fields are solved simultaneously, taking into account their coupling effects. The equations for the thermal field describe the heat conduction within the material, while the equations for the mechanical field describe the deformation and stress distribution. The partial coupling arises from the assumption that the temperature field changes due to thermal expansion or contraction, but the resulting mechanical deformation does not significantly affect the temperature distribution. This assumption is valid when the mechanical loads applied to the continuum are relatively small. By solving the coupled equations, it is possible to determine the temperature distribution and the resulting deformation and stress fields in a partially coupled thermoelastic system. This is important in various engineering applications where temperature changes can induce thermal stresses and strains, like in the design of structures subjected to thermal loading. Numerical methods based on

FEM are commonly used to solve partially coupled thermoelastic problems, where the governing equations are discretized and solved iteratively to obtain the desired solution. These methods allow engineers and scientists to predict and analyze the behavior of materials and structures under combined thermal and mechanical loading conditions.

4.3 Governing Equations

The governing equations of the FG plate are acquired by the virtual work principle. Based on this principle, the variation of the virtual work on the plate is zero. In simple terms, the virtual work variation of internal strain energy δL_{int} is equal to the virtual work variation of external loading δL_{ext}.

$$\begin{aligned} &\delta L = 0 \\ &\delta L_{\text{int}} - \delta L_{\text{ext}} = 0 \end{aligned} \tag{4.1}$$

In this study, there is no external loading. Therefore, the variation of the total energy for the plate is equal to the variation of virtual internal work and is obtained as:

$$\delta L = \delta L_{\text{int}} = 0 \tag{4.2}$$

The virtual work variation is computed as:

$$\delta L = \int_{V_e} \delta \varepsilon^T \sigma \mathrm{d}V \tag{4.3}$$

It worth be mentioned ε and σ are relations (3.4) and (3.11) respectively. But here, considering CUF, they are first rewritten and then replaced in the relation of (4.3).

The strain vector of Eq. (3.4), which is related to the displacement vector by linear and nonlinear geometrical matrices for the investigation of large deflection, can be represented as follows:

$$\varepsilon = (\mathbf{B}_l^{\tau i} + \mathbf{B}_{nl}^{\tau i})\, \mathbf{u}_{\tau i} \tag{4.4}$$

where

$$\mathbf{B}_l^{\tau i} = \mathbf{b}_l(F_\tau N_i) = \begin{bmatrix} F_\tau N_{i,x} & 0 & 0 \\ 0 & F_\tau N_{i,y} & 0 \\ 0 & 0 & F_{\tau,z} N_i \\ F_{\tau,z} N_i & 0 & F_\tau N_{i,x} \\ 0 & F_{\tau,z} N_i & F_\tau N_{i,y} \\ F_\tau N_{i,y} & F_\tau N_{i,x} & 0 \end{bmatrix} \tag{4.5}$$

$$\mathbf{B}_{nl}^{\tau i} = \frac{1}{2} \begin{bmatrix} u_{x,x} F_\tau N_{i,x} & u_{y,x} F_\tau N_{i,x} & u_{z,x} F_\tau N_{i,x} \\ u_{x,y} F_\tau N_{i,x} & u_{y,y} F_\tau N_{i,x} & u_{z,y} F_\tau N_{i,x} \\ u_{x,z} F_{\tau,z} N_i & u_{y,z} F_{\tau,z} N_i & u_{z,z} F_{\tau,z} N_i \\ u_{x,x} F_{\tau,z} N_i + u_{x,z} F_\tau N_{i,x} & u_{y,x} F_{\tau,z} N_i + u_{y,z} F_\tau N_{i,x} & u_{z,x} F_{\tau,z} N_i + u_{z,z} F_\tau N_{i,x} \\ u_{x,y} F_{\tau,z} N_i + u_{x,z} F_\tau N_{i,y} & u_{y,y} F_{\tau,z} N_i + u_{y,z} F_\tau N_{i,y} & u_{z,y} F_{\tau,z} N_i + u_{z,z} F_\tau N_{i,y} \\ u_{x,x} F_\tau N_{i,y} + u_{x,y} F_\tau N_{i,x} & u_{y,x} F_\tau N_{i,y} + u_{y,y} F_\tau N_{i,x} & u_{z,x} F_\tau N_{i,y} + u_{z,y} F_\tau N_{i,x} \end{bmatrix} \tag{4.6}$$

The variation of Eq. (4.4) is as follows:

$$\delta\varepsilon = (\mathbf{B}_l^{sj} + 2\mathbf{B}_{nl}^{sj})\,\delta\mathbf{u}_{sj} \tag{4.7}$$

It should be noted by substituting the s and j respectively, instead of τ and i in Eqs. (4.5) and (4.6) matrices $\mathbf{B}_l^{sj}$ and $\mathbf{B}_{nl}^{sj}$ are created. In this thesis, i and j are related to element nodes in the shape function, while indexes τ and s refer to expansion functions.

By replacing Eq. (4.4) in Eq. (3.11) and by substituting the resulting equation and Eq. (4.7) in Eq. (4.3), the virtual strain energy for the fundamental nucleus (FN) is rephrased as:

$$\begin{aligned} \delta L &= \int_{V_e} \delta u_{sj}^T (\mathbf{B}_l^{sj} + 2\mathbf{B}_{nl}^{sj})^T \mathbf{C}((\mathbf{B}_l^{\tau i} + \mathbf{B}_{nl}^{\tau i})\,\mathbf{u}_{\tau i} - \alpha\Delta T) dV \\ &= \int_{V_e} [\delta u_{sj}^T (\mathbf{B}_l^{sj} + 2\mathbf{B}_{nl}^{sj})^T \mathbf{C}(\mathbf{B}_l^{\tau i} + \mathbf{B}_{nl}^{\tau i})\,\mathbf{u}_{\tau i} \\ &\quad - \delta u_{sj}^T (\mathbf{B}_l^{sj} + 2\mathbf{B}_{nl}^{sj})^T \mathbf{C}\alpha\Delta T)] dV \\ &= \delta\mathbf{u}_{sj}^T \mathbf{K}_S^{ij\tau s} \mathbf{u}_{\tau i} - \delta\mathbf{u}_{sj}^T \mathbf{P}^{sj} = 0 \end{aligned} \tag{4.8}$$

Therefore, the nonlinear equilibrium equation of the FG plate under thermal load can be expressed in a unified form as follows:

$$\mathbf{K}_S^{ij\tau s} \mathbf{u}_{\tau i} = \mathbf{P}^{sj} \tag{4.9}$$

In which $\mathbf{P}^{sj}$ and $\mathbf{K}_S^{ij\tau s}$ are FN of thermal load vector and secant stiffness matrix, respectively. It can be stated each is constituted of some linear and nonlinear terms as below:

$$\mathbf{K}_S^{ij\tau s} = \mathbf{K}_0^{ij\tau s} + \mathbf{K}_{lnl}^{ij\tau s} + \mathbf{K}_{nll}^{ij\tau s} + \mathbf{K}_{nlnl}^{ij\tau s} \tag{4.10}$$

$$\mathbf{P}^{sj} = \mathbf{P}_l^{sj} + \mathbf{P}_{nl}^{sj} \tag{4.11}$$

It should be mentioned that $\mathbf{K}_0^{ij\tau s}$ is the linear FN of secant stiffness matrix while $\mathbf{K}_{lnl}^{ij\tau s}$ and $\mathbf{K}_{nll}^{ij\tau s}$ stand for first-order nonlinear FN of secant stiffness matrix, and $\mathbf{K}_{nlnl}^{ij\tau s}$ represent second-order nonlinear FN of secant stiffness matrix [45] as:

$$\begin{aligned}
\mathbf{K}_0^{ij\tau s} &= \int_{V_e} (\mathbf{B}_l^{sj})^T \mathbf{C} \mathbf{B}_l^{\tau i} dV \\
\mathbf{K}_{lnl}^{ij\tau s} &= \int_{V_e} (\mathbf{B}_l^{sj})^T \mathbf{C} \mathbf{B}_{nl}^{\tau i} dV \\
\mathbf{K}_{nll}^{ij\tau s} &= 2 \int_{V_e} (\mathbf{B}_{nl}^{sj})^T \mathbf{C} \mathbf{B}_l^{\tau i} dV \\
\mathbf{K}_{nlnl}^{ij\tau s} &= 2 \int_{V_e} (\mathbf{B}_{nl}^{sj})^T \mathbf{C} \mathbf{B}_{nl}^{\tau i} dV
\end{aligned} \tag{4.12}$$

The details of the aforementioned relations are described in Appendix.

Also, $\mathbf{P}_l^{sj}$ and $\mathbf{P}_{nl}^{sj}$ are, respectively, the linear and nonlinear FN of the load vector. According to Eq. (4.8), these are defined as:

$$\begin{aligned}
\mathbf{P}_l^{sj} &= \int_{V_e} (\mathbf{B}_l^{sj})^T \mathbf{C} \alpha \Delta T dV \\
\mathbf{P}_{nl}^{sj} &= 2 \int_{V_e} (\mathbf{B}_{nl}^{sj})^T \mathbf{C} \alpha \Delta T dV
\end{aligned} \tag{4.13}$$

By four looping on indexes i, j, τ, s of FN for secant stiffness matrix and thermal load vector, the element's stiffness matrix and thermal load vector are acquired [13]. Then they would be assembled based on the classical manner of FEM to equilibrium equation for the whole of the FG plate. For further comprehension, the process of assembling from the FN of stiffness matrix to the structure's stiffness matrix is shown in Fig. 4.1.

According to the above explanation, the governing equation for the FG plate is represented as:

$$\mathbf{K}_S \mathbf{u} - \mathbf{P} = \mathbf{0} \tag{4.14}$$

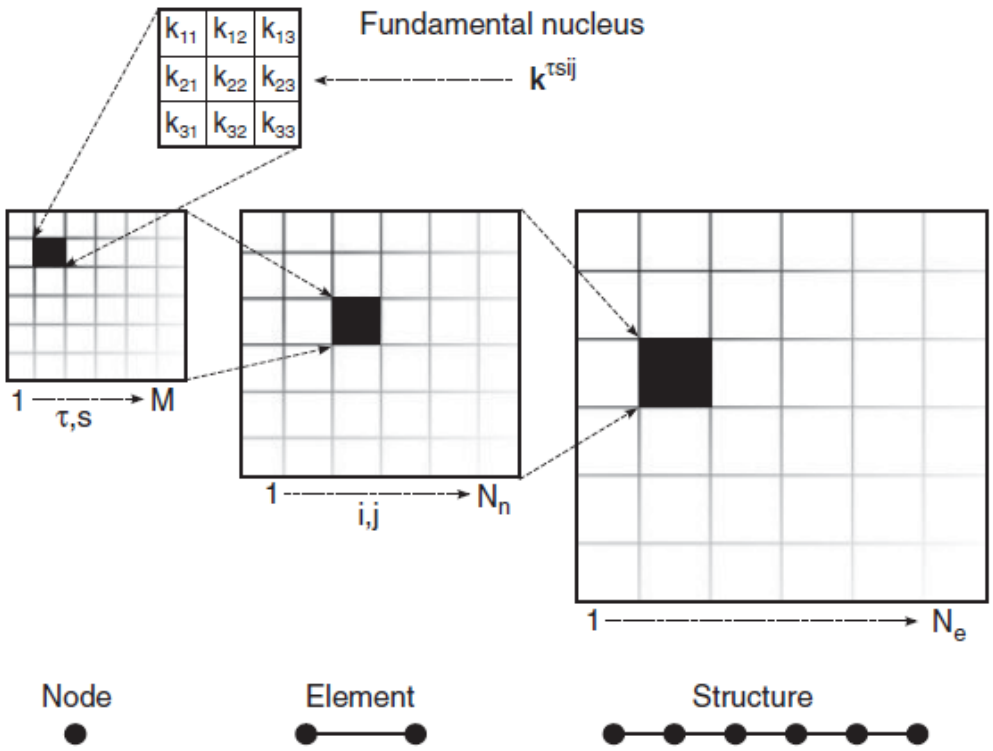

Fig. 4.1 The process of assembling the stiffness matrix[3]

In which $\mathbf{K}_S$, $\mathbf{u}$, and $\mathbf{P}$ are the total secant stiffness matrix, the total displacement, and the total thermal load vector of the FG plate. To analyze the thermal post-buckling of the FG plate, the governing equation due to nonlinear geometric must be solved. Since Eq. (4.14) is a nonlinear geometrical system, it is generally solved via incremental methods such as Newton-Raphson and arc-length. In this regard, the nonlinear equilibrium equation must be linearized.

4.4 Linearization and Jacobian matrix

In structural engineering, the Jacobian matrix is frequently dubbed the tangent stiffness matrix since it is a slope of the load-displacement curve for an arbitrary degree of freedom. For solving nonlinear governing equation by FEM via incremental methods, the unbalanced nodal load vector of equilibrium equation is defined as:

$$\mathbf{R} = \mathbf{K}_S\mathbf{u} - \mathbf{P} = \mathbf{0} \tag{4.15}$$

where **R** is the residual nodal load vector.

As the method is an incremental strategy, it is needed to increase the amount of load from a reference value to a final value by a parameter named load factor (λ). In the current research, the following equation regulates the temperature changes explicitly and controls the thermal load implicitly:

$$\begin{aligned} T &= T_0 + \lambda (T_1 - T_0) \\ T - T_0 &= \lambda (T_1 - T_0) \\ \Delta T &= \lambda \bar{\Delta T} \end{aligned} \tag{4.16}$$

where T, T_0, and T_1, respectively, are current temperature, reference temperature, and temperature related to $\lambda = 1$.
According to Eq. (4.16), the thermal load vector can be stated as:

$$\mathbf{P} = \lambda \bar{\mathbf{P}} \tag{4.17}$$

$\bar{\mathbf{P}}$ represents the proportional loads' reference vector.

Hence, Eq. (4.15) is rewritten as:

$$\mathbf{R} = \mathbf{K}_S \mathbf{u} - \lambda \bar{\mathbf{P}} \tag{4.18}$$

By extending **R** of Eq. (4.18) around an assumed solution $(\mathbf{u}, \lambda)$ by series of Taylor and using the linearization method and skipping the higher-order terms, the following expression is generated:

$$\mathbf{R}(\mathbf{u} + \delta\mathbf{u}, \lambda + \delta\lambda) = \mathbf{R}(\mathbf{u}, \lambda) + \frac{\partial \mathbf{R}}{\partial \mathbf{u}} \delta\mathbf{u} + \frac{\partial \mathbf{R}}{\partial \lambda} \delta\lambda = \mathbf{0} \tag{4.19}$$

$$\frac{\partial \mathbf{R}}{\partial \mathbf{u}} \delta\mathbf{u} = -\frac{\partial \mathbf{R}}{\partial \lambda} \delta\lambda - \mathbf{R}(\mathbf{u}, \lambda) \tag{4.20}$$

in which $\frac{\partial \mathbf{R}}{\partial \mathbf{u}}$ is equivalent to tangent stiffness matrix ($\mathbf{K}_T$) and $\frac{\partial \mathbf{R}}{\partial \lambda} = -\bar{\mathbf{P}}$. Therefore Eq. (4.20) is rewritten as below:

$$\mathbf{K}_T \delta\mathbf{u} = \bar{\mathbf{P}} \delta\lambda - \mathbf{R} \tag{4.21}$$

It should be noted an extra equation like $f(\delta\mathbf{u},\delta\lambda)=0$ is needed for solving Eq. (4.21). There are various incremental techniques may be executed. For example, $\delta\lambda=0$ is related to the load-control method, but if $\delta\mathbf{u}=\mathbf{0}$, it means a displacement control method. However, in the present work, a path-following approach according to an arc-length method mentioned by Carrera [62] is employed here. It can follow both loads factor and displacement variations. In other words, the selected relation is $A^2=\delta\lambda^2+\delta\mathbf{u}^T\delta\mathbf{u}$ in which A is arc's length.

It should be implied that the FN of the tangent stiffness matrix $\mathbf{K}_T^{ij\tau s}$ is emanated by linearizing the nonlinear governing equation. The virtual work variation formula included the geometrical relation of strain-displacement and the constitutive equation of stress-strain. Thus both must be linearized so that it causes the tangent stiffness matrix:

$$\delta(\delta L)=\delta(\int_{V_e}\delta\varepsilon^T\sigma\mathrm{d}V)=\int_{V_e}\delta\varepsilon^T\delta\sigma\mathrm{d}V+\int_{V_e}\delta(\delta\varepsilon^T)\sigma\mathrm{d}V \tag{4.22}$$

$$\delta(\delta L)=\delta\mathbf{u}_{sj}^T\mathbf{K}_T^{ij\tau s}\mathbf{u}_{\tau i} \tag{4.23}$$

By utilizing some mathematical operations that are reported in detail by Wu et al. [45], the tangent stiffness matrix's FN is extracted as:

$$\mathbf{K}_T^{ij\tau s}=\mathbf{K}_0^{ij\tau s}+2\mathbf{K}_{lnl}^{ij\tau s}+\mathbf{K}_{nll}^{ij\tau s}+2\mathbf{K}_{nlnl}^{ij\tau s}+\mathbf{K}_\sigma^{ij\tau s} \tag{4.24}$$

in which $\mathbf{K}_0^{ij\tau s}$, $2\mathbf{K}_{lnl}^{ij\tau s}$, $\mathbf{K}_{nll}^{ij\tau s}$, and $2\mathbf{K}_{nlnl}^{ij\tau s}$ are the same as FNs as given in Eq. (4.10) which are provided in the Appendix. $\mathbf{K}_\sigma^{ij\tau s}$ is FN of the geometric stiffness matrix that is proposed below:

$$\mathbf{K}_\sigma^{ij\tau s}=K_g\mathbf{I} \tag{4.25}$$

where $\mathbf{I}$ represents the identity matrix with dimensions 3×3 and K_g is as below:

$$\begin{aligned} K_g = \int_{V_e} (&\sigma^0_{xx} F_\tau F_s N_{i,x} N_{j,x} + \sigma^0_{yy} F_\tau F_s N_{i,y} N_{j,y} + \sigma^0_{zz} F_{\tau,z} F_{s,z} N_i N_j \\ &+ \sigma^0_{xy} F_\tau F_s N_{i,x} N_{j,y} + \sigma^0_{xy} F_\tau F_s N_{i,y} N_{j,x} + \sigma^0_{xz} F_\tau F_{s,z} N_{i,x} N_j \\ &+ \sigma^0_{xz} F_{\tau,z} F_s N_i N_{j,x} + \sigma^0_{yz} F_\tau F_{s,z} N_{i,y} N_j + \sigma^0_{yz} F_{\tau,z} F_s N_i N_{j,y}) dV \end{aligned} \tag{4.26}$$

where the some thermal pre-stresses such as $\sigma^0_{xy}, \sigma^0_{xz}$, and σ^0_{yz} are zero and other are as follow [61]:

$$\sigma^0_{xx} = \sigma^0_{yy} = \sigma^0_{zz} = \sigma^0 = \frac{E\alpha\Delta T^0}{1-2\nu} \tag{4.27}$$

It can rewrite Eq. (4.26) as follows:

$$K_g = \int_{V_e} \sigma^0 (F_\tau F_s N_{i,x} N_{j,x} + F_\tau F_s N_{i,y} N_{j,y} + F_{\tau,z} F_{s,z} N_i N_j) dV \tag{4.28}$$

Like the assembling procedure of the secant stiffness matrix, the tangent stiffness matrix is assembled in some steps, including creating tangent stiffness of the FN, node, element, and total structure. It is obvious that FN is utilized for the formulation of the secant or tangent stiffness matrix and the thermal load vector related to any higher-order plate theory. It can be recognized that the FN of the tangent stiffness is a symmetric matrix. It is seen, considering to problem, the fundamental nuclei's formulation of the tangent and secant stiffness matrices will be easier if just some geometric nonlinearities are contained, like von Karman nonlinearities.

4.5 Solution procedure of the thermal post-buckling analysis

Post-buckling analysis of the structures leads to a complex nonlinear differential equation that cannot be solved analytically. In this study, in order to solve the nonlinear governing equation, the tangent stiffness matrix is used to develop the linearized iterative technique. Then, the arc-length approach is utilized, which makes the tangent stiffness matrix and unbalanced load vector update at each iteration after an increment of thermal load to extract the numerical results. They are implemented

through the following steps considering two loops (load increments with index d and equilibrium iterations with index q):

1. Input plate's geometry, boundary conditions, material properties, etc and also assume $\mathbf{R}_1^1 = \mathbf{0}$.
2. Loop over load increments ($d = 1, 2, ...$).
3. Set an arc-length value (A) to designate a search domain for answers out of a guessed initial or known solution $(\mathbf{u}_1^d, \lambda_1^d)$.
4. Loop over equilibrium iterations ($q = 1, 2, ...$).
5. Set T_0 , T_1^d and compute $T_q^d = T_0 + \lambda_q^d (T_1^d - T_0)$.
6. Compute temperature distribution through the thickness of the plate according to section 2.4 by considering $T_c = T_1^d$ and calculate temperature-dependant properties (if needed).
7. Compute tangent stiffness matrix and thermal load vector according to $\mathbf{u}_q^d, T_1^d$.
8. Calculate the residual load vector in each increment-iteration.
9. Calculate $\delta\lambda_q^d, \delta\mathbf{u}_q^d$ according to: $A^2 = (\delta\lambda_q^d)^2 + (\delta\mathbf{u}_q^d)^T \delta\mathbf{u}_q^d$
$(\delta\mathbf{u}_q^d)_I = \mathbf{K}_{Tq}^{-1}\bar{\mathbf{P}}$, $(\delta\mathbf{u}_q^d)_{II} = -\mathbf{K}_{Tq}^{-1}\mathbf{R}_q^d$, $\delta\mathbf{u}_q^d = \delta\lambda_q^d(\delta\mathbf{u}_q^d)_I + (\delta\mathbf{u}_q^d)_{II}$.
10. Check if $||\delta\mathbf{u}_q^d||/||\mathbf{u}_q^d||$ and $|\delta\lambda_q^d|/|\lambda_q^d|$ are less than the convergence error tolerance? If yes, break equilibrium iteration loop, else, evaluate the below equations and go to step 4:
$\mathbf{u}_{q+1}^d = \mathbf{u}_q^d + \delta\mathbf{u}_q^d$, $\lambda_{q+1}^d = \lambda_q^d + \delta\lambda_q^d$.
11. End loop over equilibrium iterations.
12. Draw the point consisting of the desired DOF displacement (e.g. central deflection) and the corresponding temperature T_q^d.
13. Check if T_q^d has passed from a desired high temperature, break load increments loop else, consider $\mathbf{u}_1^{d+1} = \mathbf{u}_q^d$, $\lambda_1^{d+1} = \lambda_q^d$ and go to step 2.
14. End loop over load increments.
15. Connect the points extracted from step 12 together in order to obtain the path of thermal post-buckling.

4.5.1 Linear buckling analysis

It is worth mentioning that in this study, in addition to nonlinear analysis of thermal post-buckling, linear buckling analysis (LBA) also is used for getting some results and outcomes. Furthermore, there is the possibility of comparing the critical buckling temperature obtained by LBA with the bifurcation point of the thermal post-buckling path. LBA is based on the solution of an eigenvalue problem. It is a simple method for obtaining structures' buckling loads regarding the following hypotheses: (I) applying the load to the structure is conservative, and (II) nonlinear displacements are neglected. LBA just calculates the bifurcation point as a critical buckling load and cannot provide post-buckling information. The main goal of this part is to compute the critical temperature of FG rectangular plates. Although the computed eigenvalue by LBA is not a physical and real critical temperature and has little difference from the actual critical temperature, but in the design and modeling of the FG plate under uniform and nonuniform temperature distribution, the LBA approach is utilized as reliable and a low-cost method.
For solving the governing equation of the problem in order to solve by LBA, it is needed to neglect from nonlinear terms tangent stiffness matrix:

$$\mathbf{K}_T = \mathbf{K}_0 + \mathbf{K}_\sigma \tag{4.29}$$

where $\mathbf{K}_0$ and $\mathbf{K}_\sigma$ are assembled forms of $\mathbf{K}_0^{ij\tau s}$ and $\mathbf{K}_\sigma^{ij\tau s}$, respectively.

The governing equation of the FG plate in order to solve by LBA can be represented as follow:

$$\mathbf{K}_T\mathbf{u} = 0 \tag{4.30}$$

In the LBA, if the problem is temperature independent, the Eq. (4.28) can be rewritten as:

$$K_g = \beta K_G \tag{4.31}$$

where $K_G = \int_{V_e} \frac{E\alpha}{1-2\nu}(F_\tau F_s N_{i,x} N_{j,x} + F_\tau F_s N_{i,y} N_{j,y} + F_{\tau,z} F_{s,z} N_i N_j) dV$.

Consequently, assuming $\mathbf{K}_G^{ij\tau s} = K_G\mathbf{I}$, the geometric stiffness matrix for the case of temperature-independent properties would be as below:

$$\mathbf{K}_\sigma = \beta\mathbf{K_G} \tag{4.32}$$

where $\mathbf{K_G}$ is assembled form of $\mathbf{K}_G^{ij\tau s}$.

By substituting Eq. (4.32) in Eq. (4.29), and then by substituting the resulting equation in Eq. (4.30), the governing equation of the plate in order to compute critical buckling loads will be as following eigenvalue problem:

$$\mathbf{K}_0\mathbf{u} = -\beta\mathbf{K_G}\mathbf{u} \tag{4.33}$$

where $\mathbf{u}$ and β are, respectively, eigenvectors and eigenvalues. The smallest eigenvalue is known as critical buckling temperature.

If the problem depends on temperature, Eq. (4.30) can be rewritten as below:

$$\mathbf{K}_T(T)\mathbf{u} = 0 \tag{4.34}$$

Since it is temperature-dependent, it cannot be solved in a direct way as a common eigenvalue problem. It will be solved by using the successive linear problems (SLP) method [63]. This method uses two first terms of the Taylor series at T_1 (guessed initial temperature of ceramic) in order to convert Eq. (4.34) to the following equation:

$$(\mathbf{K}_T(T_1) + (T_c - T_1) \times \mathbf{K'}_T(T_1).\mathbf{u} = 0 \tag{4.35}$$

Then, by assuming $\beta = T_c - T_1$, Eq. (4.35) is rewritten as follows:

$$\mathbf{K}_T(T_1).\mathbf{u} = -\beta\mathbf{K'}_T(T_1).\mathbf{u} \tag{4.36}$$

Eq. (4.36) is a kind of eigenvalue problem, and the smallest eigenvalue of β is known as critical temperature differences.
The algorithm of the SLP method to obtain the critical temperature of ceramic is as below:

1. Input mechanical and thermal properties, plate's geometry, boundary conditions, etc

2. Guess the initial ceramic's temperature $T_1 = 10\,K$
3. Calculate material properties based on T_1
4. Calculate tangent stiffness matrix based on T_1
5. Calculate derivative stiffness matrix based on T_1 using finite difference $\mathbf{K}'_T(T_1) = \frac{\mathbf{K}_T(T_1+dT)-\mathbf{K}_T(T_1)}{dT}$ (e.g. $dT = 0.1K$)
6. Solve $|\mathbf{K}_T(T_1) + \beta \mathbf{K}'_T(T_1)| = 0$ to get β
7. $T_c = T_1 + \beta$
8. If $T_c - T_1 < \varepsilon$ then go to step 10, else go to step 9
9. Input the value of T_c into T_1 and go to step 3
10. Write T_c as critical temperature of ceramic (T_c^{cr})

Chapter 5

Numerical examples and discussion

5.1 Introduction

In this chapter, several numerical examinations are reported to indicate the capability of the proposed method based on CUF using FEM to analyze the FG plate's thermal buckling loads and thermal post-buckling response. In other words, in section 5.2, the figures and tables are presented to demonstrate the critical temperature value of the FG plate in different conditions. In the figures of section 5.3 related to thermal post-buckling, the temperature curve was drawn versus the central deflection of the FG plate. In this chapter, the results are obtained with and without considering the properties' dependency on temperature so that TD shows temperature-dependent properties, while TID means properties are temperature-independent. In some examples, the properties of the plate are TD, while others have TID properties. Also, they are subjected to uniform and nonuniform temperature distribution through the thickness. Furthermore, in some examples, LBA in the thermal environment has been done to compare its results with bifurcation points extracted by thermal post-buckling analysis. In order to validate, the thermal post-buckling of FG plates' behavior using the current method is compared with similar references. Parametric studies are taken to demonstrate the effect of geometrical dimensions, volume fraction index, type of FGM combination and boundary conditions on the thermal buckling and post-buckling response of the rectangular FG Plate.

5.2 Thermal buckling load of FG rectangular plates

In this section, a number of numerical examples are presented using LBA. The behavior of thermal buckling loads of FG plates under heat load with uniform and nonuniform distributions in the direction of thickness is investigated. Here, two types of materials combination have been used for analyzing the FG plate. One of them is Nickel/Silicon Nitride (Ni/Si_3N_4), and another is Titanium/Zirconium Oxide alloy ($Ti-6Al-4V/ZrO_2$). It should be noted that in obtaining the results of Tables 5.1 to 5.5, and Figures (5.2) and (5.3), the combination of (Ni/Si_3N_4) has been used. In reaching the results of Tables 5.6 and 5.7, and also Figures (5.4) and (5.5), the combination of ($Ti-6Al-4V/ZrO_2$) has been utilized.

The results of the examples by considering the metal's temperature equal to $0\,K$, various volume fraction indexes, and different boundary conditions have been extracted by utilizing FEM based on CUF. Figure (5.1) investigates the sensitivity of the critical temperature to expansion order on the FG plates with $a/b=2$, $a/t=100$, and $n=10$. From Figure (5.1), it is clear that the critical temperature of the FG plates is converged to a definite value for expansion order equal to 3 and upper than it. So, the value of expansion order is selected equal to 3 for reducing computational costs in getting results. This selection reduces not only computational costs but also has high accuracy.

Sensitivity analysis on volume fraction index, length to width ratio a/b, length to thickness ratio a/t, temperature distribution, and type of boundary conditions have also been performed. In order to compare and validate, Tables 5.1 to 5.4 are presented. In Tables 5.1 and 5.2, the results have been computed based on uniform temperature distribution and they have been compared with the results of reference [24]. It should be noted in Tables 5.1 and 5.2, the results have been expressed in terms of dimensionless temperature $\bar{T}_c^{cr}=\alpha_0 T_c^{cr}\times 10^3$. In which α_0 is calculated based on Nickle thermal expansion coefficient at $300\,K$ according to material properties of Table 2.1.

In Tables 5.3 and 5.4, the results of the present study are extracted by using the temperature distribution already explained in section 2.4 and have been compared with the results obtained by assumed nonuniform temperature distribution in reference [4]. It must be mentioned assumed temperature profile of reference [4] is approximated as follow:

$$T(z) = (T_c - T_m)(\frac{z}{t} + \frac{1}{2})^{\gamma} + T_m \tag{5.1}$$

As mentioned in reference [4], in Eq. (5.1), γ is an index when it is equal to 1, it supposes a linear distribution and when it is equal and higher than 2, it means the order of nonlinearity temperature distribution. Tables 5.1 and 5.2 show the critical temperature of rectangular FG plates under uniform temperature distributions, while the data of 5.3 and 5.4 are related to critical temperatures based on nonuniform temperature distributions. By paying attention to Tables 5.1 and 5.2, it can be found there are some differences between the results of the present study and the results of reference [24]. These differences are due to the theory being used in each of them. The present study's results are more accurate because a higher-order theory, CUF, is applied, and in reference [24], FSDT has been utilized.

It is shown in reference [51] that the higher the power of the expansion function, the lower the critical load and the more accurate the result. Tables 5.3 and 5.4 prove the accuracy of the results of the present study that are extracted by the exact temperature distribution in comparison with a nonuniform assumed temperature distribution. As shown in Tables 5.3 and 5.4, in columns of reference [4], instead of decreasing the critical temperature by increasing the amount of power of the assumed temperature distribution, it increases. In all states, the critical temperature of the present study is different from the results of reference [4], and only for the power of 1, it has an amount relatively close to the results of reference [4]. It means that the present study results are remarkably accurate because the critical temperatures of the present study have resulted from the temperature distribution calculated by solving the heat conduction equation using FEM. Figure (5.2) is given to understand this matter better.

According to Figure (5.2), it can be understood that the temperature distribution in the FG plate has an influential role in obtaining correct and accurate results. Ceramic's critical temperature is not conventional for the nonlinear state ($\gamma = 2,3$) of the assumed temperature distribution of reference [4] and differs significantly from its corresponding value, which is calculated using the temperature distribution described in the section 2.4.

According to Table 5.5, the critical temperature with supposing dependency of properties to temperature for higher a/b is significantly less than the critical temperature received without the assumption of temperature-dependent properties compared to lower a/b. Results of Tables 5.6 and 5.7 have been extracted considering CCCC

and SSSS boundary conditions, respectively. From these tables, it can be discovered that the critical temperature obtained considering the dependency of properties to temperature for lower a/t has more difference with the critical temperature resulting without considering temperature-dependent properties.

Figures (5.3) and (5.4) illustrate the effects of a/t and a/b on the critical temperature of the simply supported rectangular FG plate for both types of materials combination in TD and TID states. It is clear from Figures (5.3) and (5.4) that the critical temperature decreases with increasing a/t although it grows with raising a/b with or without considering dependency on temperature. It is seen from Figure (5.3), in the square plate ($a/b = 1$), for various volume fraction indexes, the critical temperature values related to all volume fraction indexes are closer to each other. On the contrary, for high a/b, the values of the critical temperature are far from each other for them. It can be seen the geometry of the plate affects the critical temperature. It is also apparent from Figure (5.4) that in the state $a/t = 100$, the critical temperature values are near together for different volume fraction indexes. On the other side, for $a/t = 40$, they exist distant from each other for various volume fraction indexes. It can be realized the plate's thickness influences the critical temperature directly.

Results of critical temperature versus boundary condition are also shown in Figure (5.5). From this diagram, it can be caught that the critical temperature for CCCC boundary conditions is much higher than SSSS. It also can be recognized that in the case of TD properties, the critical temperature for the lowest a/t, has more difference with the critical temperature extracted with TID properties in comparison with maximum a/t that both cases have the near result.

According to Figure (5.6), increasing the volume fraction index in Ni/Si_3N_4 reduces the critical temperature, although in $Ti-6Al-4V/ZrO_2$ the critical temperature has been increased. Therefore, the type of combinations of materials (here $Ti-6Al-4V/ZrO_2$ or Ni/Si_3N_4) has an evident influence on the critical temperatures in analyzing the behavior of the thermal buckling loads. One of the fundamental reasons for the difference in behavior shown in Figure (5.6) is due to the difference in thermal conductivity coefficients. Since the calculation of the temperature distribution depends on the thermal conductivity coefficient of the materials used in the plate, the resulting critical temperature is also affected by the materials used in the plate. According to Table 2.1, it can be seen that Ni has a thermal conductivity coefficient approximately 187 times greater than $Ti-6Al-4V$ (both used as metal in FG plate),

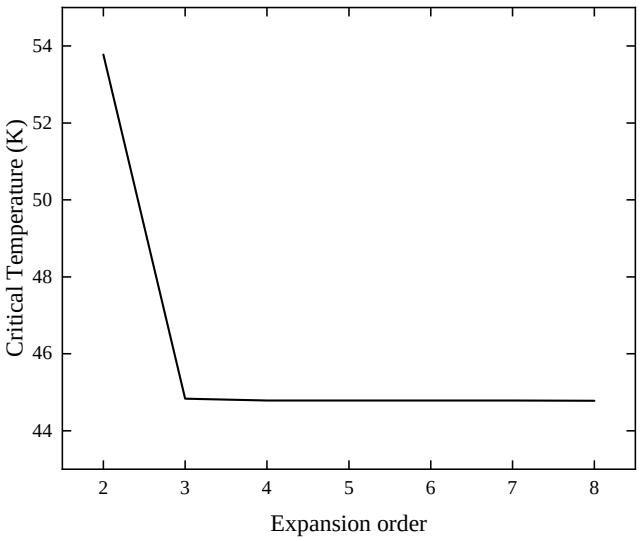

Fig. 5.1 Sensitivity of the critical temperature to expansion order.

and also, the thermal conductivity coefficient of Si_3N_4 is around eight-fold than the thermal conductivity coefficient of ZrO_2 (both used as ceramics in FG plate).

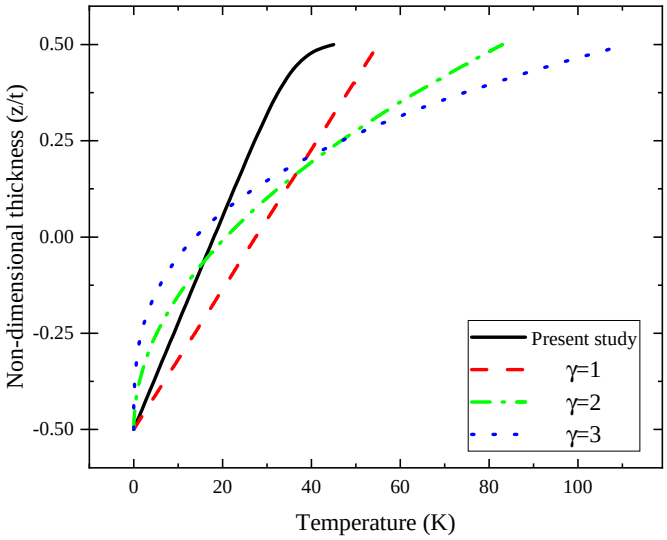

Fig. 5.2 Comparing critical temperature profile of present study with critical temperature profiles of reference [4].

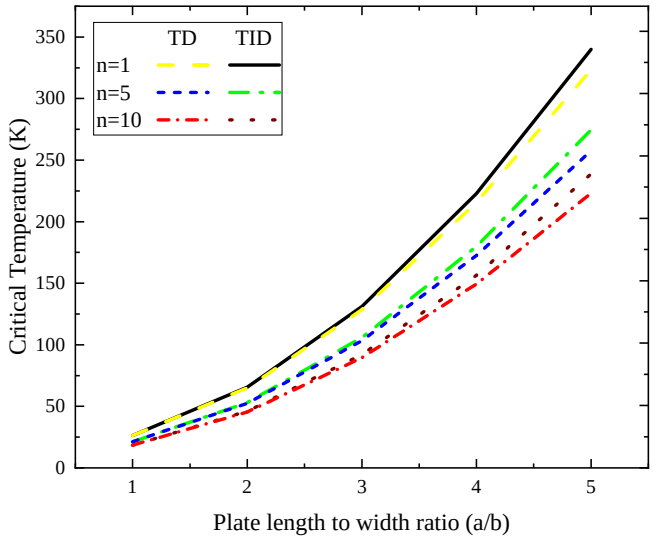

Fig. 5.3 critical temperature versus a/b.

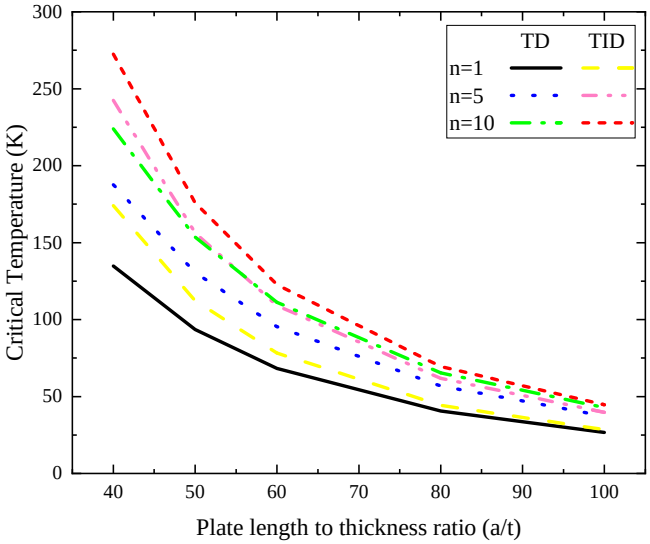

Fig. 5.4 critical temperature versus a/t.

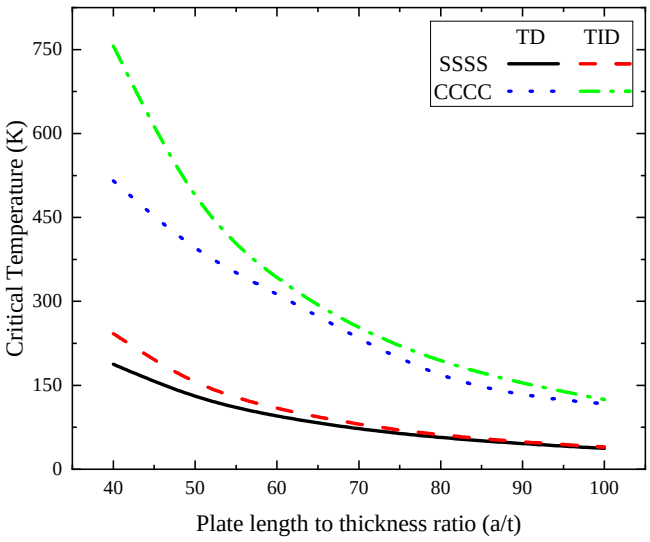

Fig. 5.5 Sensitivity of the critical temperature to boundary conditions.

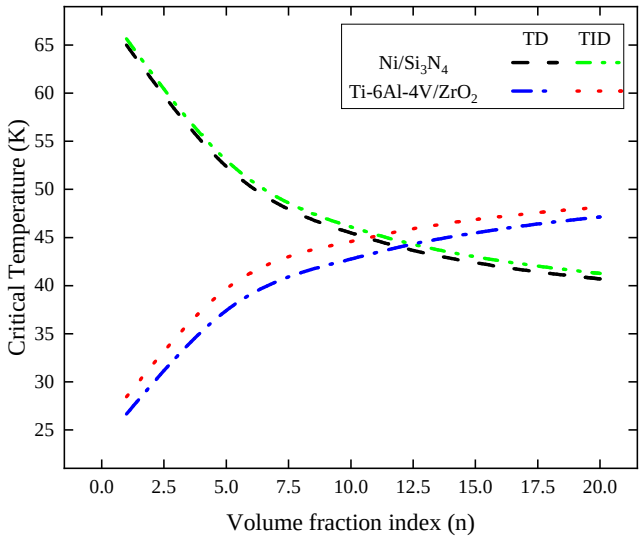

Fig. 5.6 Sensitivity of the critical temperature to kind of compositions of metal and ceramic.

Table 5.1 Non-dimensional critical temperature of ceramic $\bar{T}_c^{cr}$ for clamped rectangular FG plate under uniform temperature rise with $a/t = 30$

	$a/b = 1$		$a/b = 1.5$	
n	reference [24]	present study	reference [24]	present study
0(TID)	14.087	11.7871	24.342	20.433
0(TD)	4.9867	3.6472	7.6920	7.0151
0.5(TID)	6.9458	5.8061	7.3584	7.3407
0.5(TD)	4.0583	3.6019	5.7121	5.1353
2(TID)	4.8657	3.8841	6.6275	5.6379
2(TD)	3.6595	3.5700	5.3330	5.0229
10(TID)	4.0680	3.0798	6.1479	5.3480
10(TD)	3.4825	2.5060	5.0544	4.7613

Table 5.2 Non-dimensional critical temperature of ceramic $\bar{T}_c^{cr}$ for clamped rectangular FG plate under uniform temperature rise with $a/t = 50$

	$a/b = 1$		$a/b = 1.5$	
n	reference [24]	present study	reference [24]	present study
0(TID)	5.1235	4.3008	8.9186	7.5208
0(TD)	2.0828	1.1518	3.3981	1.9223
0.5(TID)	2.5260	2.1194	2.7082	2.7021
0.5(TD)	1.6609	1.0585	2.4112	1.7256
2(TID)	1.7712	1.4186	2.4366	2.0756
2(TD)	1.4798	1.0232	2.2433	1.6759
10(TID)	1.4822	1.1254	2.2584	1.7862
10(TD)	1.3976	0.9859	2.1208	1.6565

Table 5.3 Critical temperature of ceramic T_c^{cr} (K) for simply supported rectangular FG plate under nonuniform temperature rise with $a/t = 100$, $a/b = 1$

	present	reference [4]		
n	study	$\gamma = 1$	$\gamma = 2$	$\gamma = 3$
1(TID)	26.3231	26.5427	40.4946	54.6340
1(TD)	26.2156	26.0534	39.3628	52.5968
5(TID)	21.2627	23.1963	35.0739	47.1168
5(TD)	21.1542	22.8337	34.2457	45.6291
10(TID)	18.4906	22.1893	33.4279	44.7616
10(TD)	18.3880	21.8604	32.6844	43.4337

Table 5.4 Critical temperature of ceramic T_c^{cr} (K) for simply supported rectangular FG plate under nonuniform temperature rise with $a/t = 100$, $a/b = 2$

	present	reference [4]		
n	study	$\gamma = 1$	$\gamma = 2$	$\gamma = 3$
1(TID)	65.6657	66.3241	101.186	136.5199
1(TD)	65.0067	63.4233	94.6109	124.9215
5(TID)	53.0319	57.9562	87.6394	117.7241
5(TD)	52.3638	55.7939	82.8042	109.1654
10(TID)	46.1127	55.4405	83.5218	111.8337
10(TD)	45.4818	53.4753	79.1692	104.1843

Table 5.5 Critical temperature of ceramic T_c^{cr} (K) for simply supported rectangular FG plate under nonlinear temperature rise with $a/t = 40$ versus various a/b

	a/b			
n	1	2	3	4
1(TID)	161.8037	401.7035	799.0625	1344.370
1(TD)	157.9325	378.7939	709.3272	1208.750
5(TID)	130.5942	324.1648	644.8110	1084.777
5(TD)	126.6398	300.9130	558.4389	952.8177
10(TID)	113.5635	281.8798	560.7076	943.3746
10(TD)	109.8452	260.3532	482.8028	828.3657

Table 5.6 Critical temperature of ceramic T_c^{cr} (K) for clamped rectangular FG plate under nonlinear temperature rise with $a/b = 2$ versus various a/t

	a/t			
n	40	60	80	100
0(TID)	387.2542	175.2887	99.2891	63.7754
0(TD)	295.4867	143.6808	90.9303	62.0161
1(TID)	541.8506	245.2940	138.9478	89.2507
1(TD)	447.4807	226.4899	120.9446	83.1542
5(TID)	756.1984	342.7639	194.2473	124.7968
5(TD)	515.3181	312.9343	169.0928	116.6659
10(TID)	852.3991	386.3836	218.9704	140.6817
10(TD)	650.6272	320.3245	201.8116	125.9099

Table 5.7 Critical temperature of ceramic T_c^{cr} (K) for simply supported rectangular FG plate under nonlinear temperature rise with $a/b = 2$ versus various a/t

	a/t			
n	40	60	80	100
0(TID)	123.3975	55.5362	31.4130	20.1656
0(TD)	100.8262	50.2977	29.6472	19.4195
1(TID)	174.0401	78.3455	44.3184	28.4514
1(TD)	134.8174	68.1983	40.5270	26.6558
5(TID)	242.4470	109.1992	61.7855	39.6697
5(TD)	187.6369	95.4530	56.8312	37.4085
10(TID)	272.5469	122.7489	69.4501	44.5901
10(TD)	223.8799	111.1412	65.3453	42.7467

5.3 Thermal post-buckling analysis of FG rectangular plates

The significance and benefit of the current method in the prediction of the thermal post-buckling response of rectangular FG plates are determined in this part. Here, the FG plate has been examined considering two different types of combinations of materials. One compound is Nickel/Alumina (Ni/Al_2O_3), and another is Stainless Steel and Silicon Nitride ($SUS304/Si_3N_4$). The results of Figures (5.7) to (5.12) and Table 5.8, have been obtained based on the FG plate made from (Ni/Al_2O_3), and in Figures (5.13) to (5.15) have been acquired by considering ($SUS304/Si_3N_4$) for the FG plate. Their material properties are expressed in Tables 2.1 and 2.2.
In this section, in all figures, the temperature path is drawn versus the central deflection of the FG plate. Sensitivity analysis on the geometric ratios such as length to width a/b and length to thickness a/t, type of boundary condition, type of temperature distribution, dependency or independency to temperature, and volume fraction index have been investigated for the thermal post-buckling analysis of the FG plates. In examples of this part, the volume fraction index and the reference temperature are equal to $n = 1$ and $290K$, respectively, unless it has stated another value in some particular cases. In this study, everywhere it has been mentioned about nonuniform temperature, it means that it is computed according to section 2.4.
In Figures (5.7) to (5.12), and Table 5.8, the results have been presented in terms of non-dimensional temperature $\hat{T} = (\alpha_c + \alpha_m)\, T \times 10^3$. It should be mentioned in Figures (5.7) to (5.11), and Table 5.8, the boundary condition of the FG plate is CCCC. From Fig. (5.7), it is evident that the FG plates' thermal post-buckling path has converged to a specific order of expansion equal to 3 and higher than it. Thus, in all examples of this section, the value of 3 is selected as expansion order, not only for reducing computational costs but also for high accuracy in getting results.
Figures (5.8) and (5.9) show the temperature-deflection curves of the FG plate for various a/t by considering $a/b = 1$ under uniform and non-uniform temperature distribution, respectively. According to Fig. (5.8) and Fig. (5.9), it can be found the current method is validated with similar Ref. [5] for both cases of uniform and nonuniform temperature distribution. Since the temperature value in exchange for each central deflection of the plate is lower than the corresponding reference value, this proves that the present method is more accurate. Furthermore, it can be seen the reduction of a/t causes a lowering of the FG plate's deflection. Also, it is

evident the plate is buckled later for lower a/t. It means that the critical temperature for the inferior a/t has a higher value in comparison to the greater a/t. Hence, when a/t reduces, the FG plate acts as a thick plate, making it stiffer versus rising temperatures.

Fig. (5.10) displays the path of temperature-deflection for various a/b regarding $a/t = 100$ under uniform and nonuniform temperature distribution. From the figure, it can be seen the rise of a/b yields sooner buckling of the FG plate. In other words, the increment of a/b induces more deflection on the FG plate. However, by paying attention to Fig. (5.10), for $a/b = 20$, it cannot find an exact bifurcation point, but for $a/b = 1$ and $a/b = 10$, the bifurcation point is more visible. It should be mentioned the increase of a/b causes more deflection in FG plates for both cases of uniform and nonuniform temperature distribution. Also, it can be understood in the same aspect ratio, the FG plate subjected to non-uniform temperature distribution has a higher buckling temperature in comparison to the case under the uniform temperature distribution.

Fig. (5.11) demonstrates the influences of the volume fraction index on FG plates' temperature-deflection curve under the nonuniform temperature profile. It makes sense that the deflection of the fully ceramic plate is lower than that of the rich metal under the same thermal load. In other words, in this study, the FG plate evolves much stiffer versus a weak value of the volume fraction index because the FG plate's flexural rigidity is high.

In Fig. (5.12), three types of boundary conditions are assessed under both uniform and nonuniform temperature distribution. The first case is CCCC; the second type is SSSS; and the third one includes two parallel clamped and two parallel simply supported edges (CSCS). It can be recognized that the SSSS causes more deflection than the CSCS under the same temperature distribution and same thermal load. In addition, in both SSSS and CSCS, a bifurcation point cannot be found evidently. In other words, these two cases go to the post-buckling area directly without passing from a definite point like critical buckling temperature. But in the case of CCCC, a critical buckling point can be seen clearly on the path of the temperature-deflection; then, it inputs to the post-buckling region. As anticipated, the plate with CCCC boundary conditions has the most inferior deflection for low temperatures. Nonetheless, this case reacts inversely to high temperatures, and the FG plate buckles more readily.

In Fig. (5.13), the thermal post-buckling path of the FG plate with $a/b = 1$, $a/t = 20$

, $n = 1$ under nonuniform temperature distribution in SSSS state for both TD and TID properties is compared with Ref. [6] as a similar work. In this part, both the present study and the reference utilized order 3 in the assumption of displacement in the thickness direction, with this difference that a TSDT function based on Reddy's theory has been applied in the reference, while in the present work, it is used in the Taylore polynomial as an expansion function based on CUF. From this Figure, it can be found the current method has more accurate results because the path of the post-buckling related to the present study is at a lower level in comparison with Ref. [6]. In addition, from Figure (5.13), it can be seen the temperature-deflection path of the FG plate by assuming TD properties is more underneath than that considering TID properties.

Figure (5.14) illustrates the thermal post-buckling path of the FG plate with $a/b = 1$, $a/t = 20$ considering TD properties for $n = 1, 10$ under two different boundary conditions: CCCC and SSSS. From this figure, it is evident that when the thermal load is applied on the plate, similar to the FG plate with TID properties, the clamped type with TD properties can tolerate up to a definite value, and after this value, it goes to post-buckling phase while the simply supported type with TD properties starts buckling from the beginning. Also, from this figure, it can be understood that increasing the volume fraction index decreases the thermal post-buckling path level for both CCCC and SSSS.

Figure (5.15) shows the temperature-deflection path of the FG plate with $a/b = 1$, $a/t = 100$, $n = 1$ for both TD and TID properties under two different boundary conditions of CCCC and SSSS. According to this Figure, although the path of thermal post-buckling related to TD properties is below the TID, since the plate is relatively thin, the result of the temperature-deflection path of TD and TID are close together. But this matter differs for the moderately thick FG plate, as seen in Figure (5.13). It means that the distance level between the path extracted by assuming TD and that TID in the thick plate is much more than the thin plate. From both Figures (5.13) and (5.15), it can be seen that for making a specific central deflection, the case of CCCC needs higher temperature rising rather than the case of SSSS. In other words, the path of temperature-deflection of the FG plate for CCCC state is always at an upper level compared to SSSS state.

In order to compare the results extracted by nonlinear analyzing of thermal post-buckling of the FG plate with results of the critical temperature obtained by LBA and also prove the present study's accuracy using CUF rather than other methods of

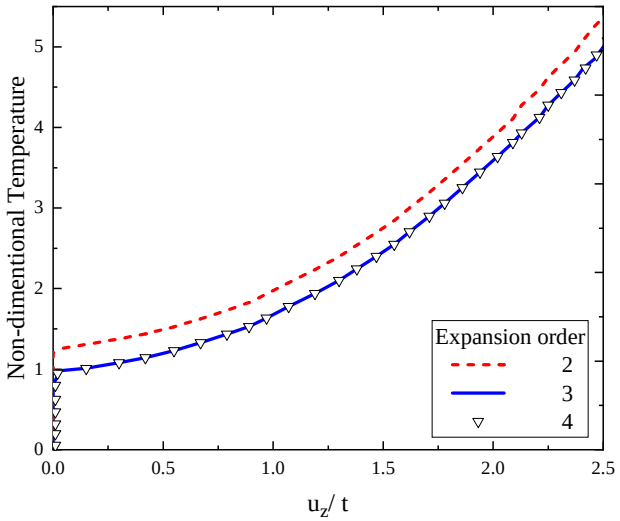

Fig. 5.7 Sensitivity analysis of thermal post-buckling path to expansion order for a clamped FG plate with $a/b = 1$ and $a/t = 100$ under the nonuniform temperature distribution

similar references, Table 5.8 is presented for a clamped rectangular FG plate with $a/b = 1$ and three different a/t. In Table 5.8, critical temperatures extracted from the thermal post-buckling path of the current method for both cases of uniform and nonuniform temperature distributions are less than that extracted from the thermal post-buckling analysis of Ref. [5]. By comparing critical temperatures values of LBA based on CUF with values of bifurcation from the present study and bifurcation of the reference, it can be understood amounts of LBA are closer to Ref.[5]. Since employing CUF in LBA have a result near the bifurcation point of post-buckling analysis without CUF, definitely applying CUF on thermal post-buckling has more accurate results, as shown in the Table. It is another proof that CUF is a powerful formulation and theory for analyzing thermal buckling and post-buckling of the plate.

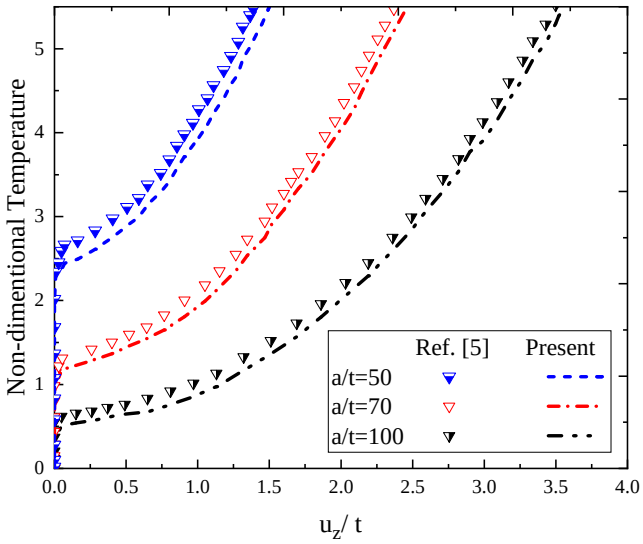

Fig. 5.8 Thermal post-buckling path of the clamped FG plate with $a/b = 1$ for various a/t under the uniform temperature distribution compared with Ref. [5]

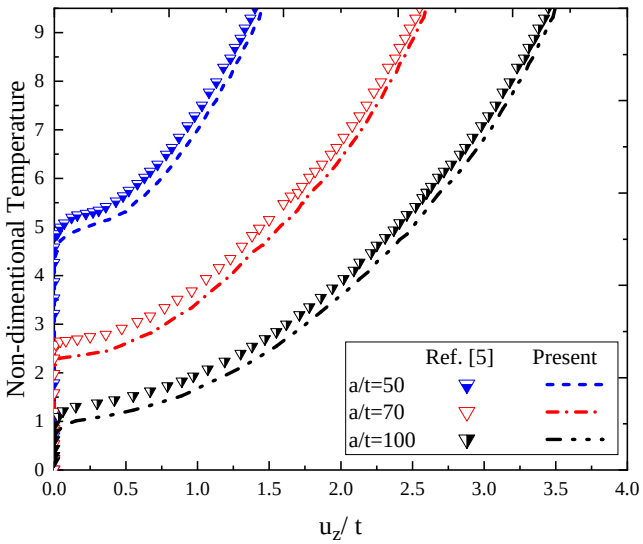

Fig. 5.9 Thermal post-buckling path of the clamped FG plate with $a/b = 1$ for various a/t under the nonuniform temperature distribution compared with Ref. [5]

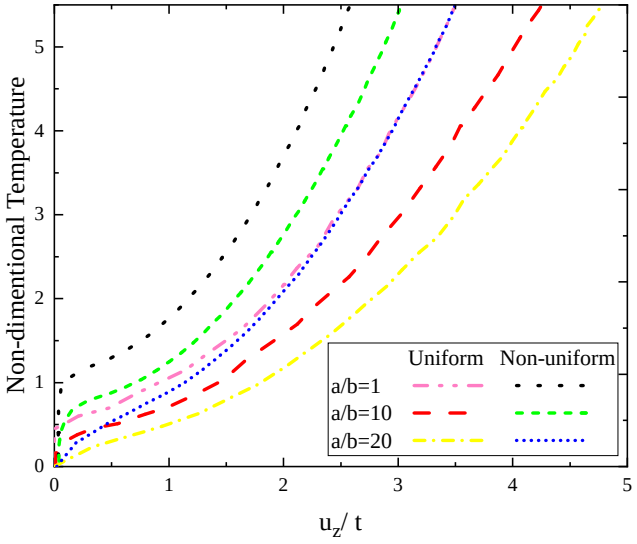

Fig. 5.10 Thermal post-buckling path of the clamped FG plate with $a/t = 100$ for various a/b under the uniform and nonuniform temperature distribution

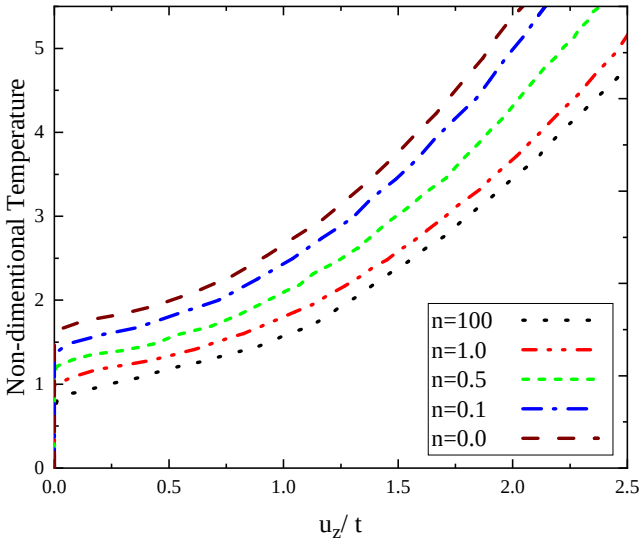

Fig. 5.11 Thermal post-buckling path of the the clamped FG plate with $a/b = 1$ and $a/t = 100$ for various volume fraction index under the nonuniform temperature distribution

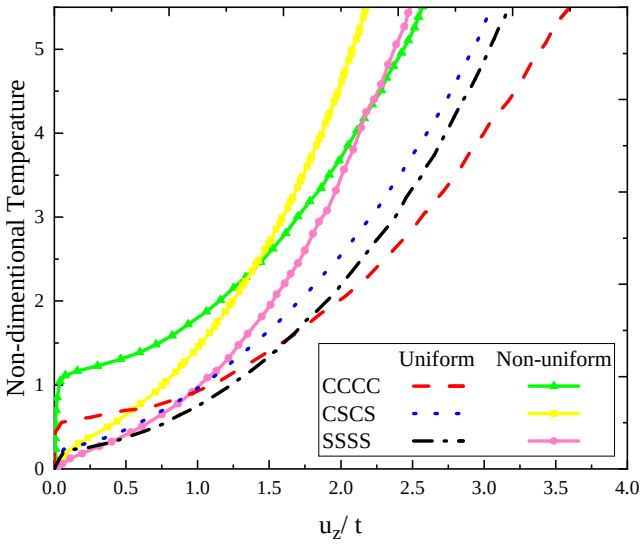

Fig. 5.12 Thermal post-buckling path of the FG plate with $a/b = 1$ and $a/t = 100$ for various boundary conditions under the uniform and nonuniform temperature distribution

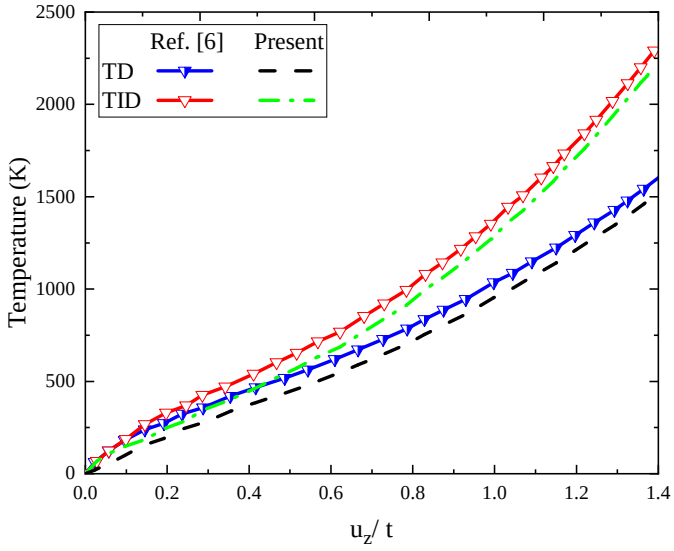

Fig. 5.13 Thermal post-buckling path of the simply supported FG plate with assuming both temperature dependent and independent properties for $a/b = 1$ and $a/t = 20$ under the nonuniform temperature distribution compared with Ref. [6]

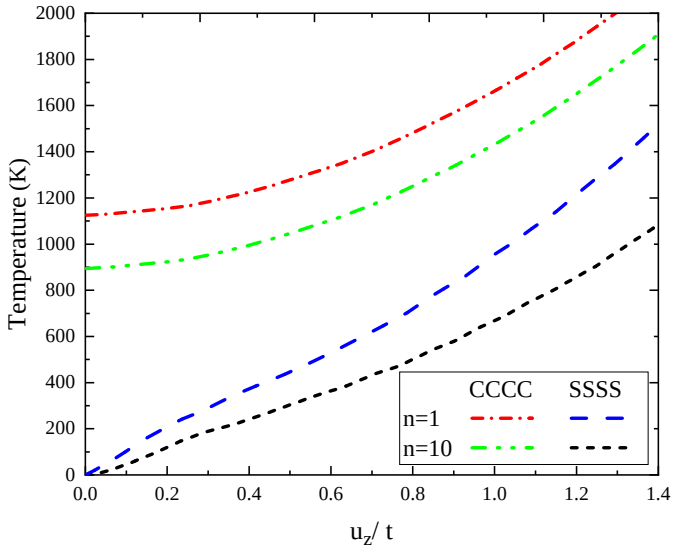

Fig. 5.14 Thermal post-buckling path of the FG plate with assuming temperature dependent properties for $a/b = 1$ and $a/t = 20$ under the nonuniform temperature distribution

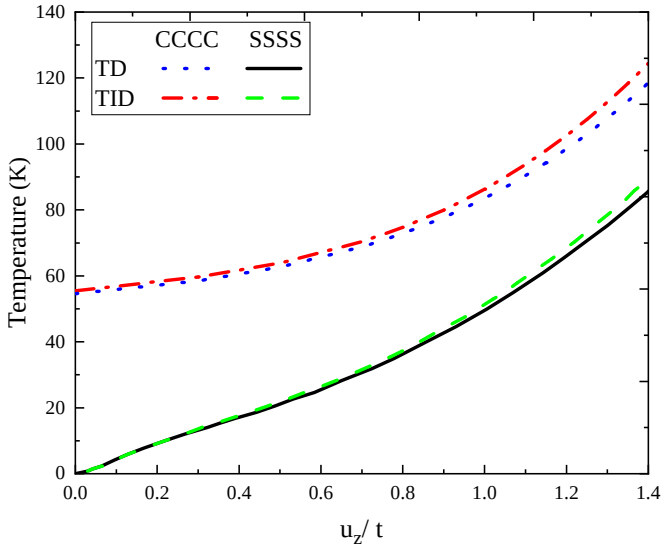

Fig. 5.15 Thermal post-buckling path of the FG plate with assuming both temperature dependent and independent properties for $a/b = 1$ and $a/t = 100$ and under the nonuniform temperature distribution

Table 5.8 Comparison of three different methods for calculating non-dimensional critical temperatures for clamped rectangular FG plates with $a/b = 1$ and various a/t

	$Uniform$			$Non-uniform$		
a/t	present study	reference [5]	LBA method	present study	reference [5]	LBA method
50	2.30	2.45	2.75	4.50	4.80	5.20
70	1.15	1.25	1.41	2.25	2.55	2.74
100	0.50	0.60	0.69	1.00	1.20	1.35

Chapter 6

Conclusions

6.1 Summary

There were three general parts for the solution of the problems in this thesis: The first part deals with utilizing LBA to determine the critical thermal buckling load for an FG plate with temperature-dependent properties. The second part is related to a nonlinear thermal post-buckling analysis of the FG plate utilizing the arc-length approach. The final part describes how to analyze the nonlinear thermal post-buckling behavior of the FG plate while taking temperature-dependent properties into account.

6.2 Conclusions

Based on the examples' results in chapter 5, the following consequences are evaluated:

1. Real temperature distribution should be used instead of assumed temperature distribution to obtain accurate results in thermal buckling problems.

2. Concerning increasing the volume fraction index, it can be found that increasing or decreasing the critical temperature difference depends on the mixture and type of ceramic and metal used in the FG plate. Because this increase in some combinations of metal and ceramic increases the critical temperature difference and reduces it in some other compounds.

3. The higher-order theory utilized in this thesis in the framework of FEM based on CUF is a very powerful theory for analyzing behavior of the thermal buckling loads of FG plates. Since the order of expansion function (Taylor-like functions) is considered 3, the results obtained from it are much closer to the actual behavior in comparison with some other theories like FSDT.

4. It must be mentioned that regardless of the type of materials combination, volume fraction index, and other parameters, the temperature-dependent properties caused a decrease in the critical temperature. So, it is better to consider the temperature-dependent properties in the behavior of the thermal buckling loads of an FG plate to obtain a more accurate result.

5. A significant result is that the effect of material dependency on temperature can be seen much more clearly on the critical temperature when a/b is too high or a/t is much low. It means, in such state, the difference value of critical temperature extracted based on TD properties with that extracted based on TID properties is at the highest.

6. In the thermal post-buckling analysis, the plate's deflection rises nonlinearly with the temperature increment. The paths of temperature-deflection prove FGM is capable of withstanding thermal loads that are induced by high-temperature differences.

7. The expansion's order of CUF theory used here is greater than FSDT, the theory utilized in the Ref. [5], that is, its DOF is higher, so its stiffness is lower and more accurate than the reference's stiffness. Therefore, its deflection is larger than the reference's deflection for the same thermal load, which better describes the post-buckling of the FG plate. In other words, the outcomes achieved from the present study are considerably closer to the real behavior of the FG plate compared with theories such as FSDT and TSDT.

8. Lengthening or thinning of the FG plate increases its deflection in the thermal post-buckling analysis under both uniform and nonuniform temperature distribution.

9. The fully clamped FG plate has a lower deflection for inferior temperatures but responds inversely to heightened temperatures and buckles more. This affair

may be described by the reality that a fully clamped plate has more constraints; thus, the plate would be so sensitive to temperature rises that influences the FG plate's stiffness.

10. Post-buckling analysis reveals that bifurcation has appeared only at aspect ratios lower than $a/b \leqslant 10$ and fully clamped boundary conditions. Besides post-buckling analysis, LBA can calculate it correctly considering these conditions.

11. The thermal post-buckling path of the FG plate is at a lower level when the TD properties are assumed than the TID properties are considered.

12. When a thermal load is imposed on the plate, the clamped FG plate with TD or TID properties can tolerate up to a certain value before entering the post-buckling phase, whereas the simply supported type properties begin to buckle right away.

13. For the FG plate with both CCCC and SSSS boundary conditions, the temperature-deflection path level reduces as the volume fraction index rises.

14. The distance level between the temperature-deflection path extracted considering TD and that extracted by TID in the thick plate is much more than the thin plate.

15. The thermal post-buckling path of the FG plate under CCCC boundary conditions is always at a higher level than under SSSS conditions.

6.3 Suggestions

According to the search in various sources to complete this thesis, the lack of the following research is felt:

1. Thermal post-buckling analysis in nanomaterials based on CUF.

2. Thermal post-buckling analysis in FG piezoelectric sandwich plates with the porous core using CUF.

3. Hygrothermal post-buckling analysis of FG plates based on CUF.

4. Experimental analysis of thermomechanical post-buckling of FG plate.

6.4 Extracted journal papers

The list of journal papers extracted from this thesis is as follows:

1. Majid Afzali, Mojtaba Farrokh and Erasmo Carrera “Thermal buckling loads of rectangular FG plates with temperature-dependent properties using Carrera Unified Formulation”, Composite Structures (2022): 295, 115787

2. Majid Afzali, Mojtaba Farrokh and Erasmo Carrera “Nonlinear thermal post-buckling analysis of rectangular FG plates using CUF”, Composite Structures (2023): 117282

References

[1] Hoang Nam Nguyen, Tran Thi Hong, Pham Van Vinh, Nguyen Dinh Quang, and Do Van Thom. A refined simple first-order shear deformation theory for static bending and free vibration analysis of advanced composite plates. *Materials*, 12(15):2385, 2019.

[2] Justin A Haught. *Aeroelasticity of Composite Plate Wings using HSDT and Higher-Order FEM*. West Virginia University, 2020.

[3] Erasmo Carrera, Fiorenzo A Fazzolari, and Maria Cinefra. *Thermal stress analysis of composite beams, plates and shells: Computational modelling and applications*. Academic Press, 2016.

[4] Vuong Nguyen Van Do and Chin-Hyung Lee. A new n th-order shear deformation theory for isogeometric thermal buckling analysis of fgm plates with temperature-dependent material properties. *Acta Mechanica*, 230(10):3783–3805, 2019.

[5] S Trabelsi, A Frikha, S Zghal, and F Dammak. Thermal post-buckling analysis of functionally graded material structures using a modified fsdt. *International Journal of Mechanical Sciences*, 144:74–89, 2018.

[6] Loc V Tran, Phuc Phung-Van, Jaehong Lee, Hung Nguyen-Xuan, and M Abdel Wahab. Isogeometric approach for nonlinear bending and post-buckling analysis of functionally graded plates under thermal environment. *arXiv preprint arXiv:1511.01380*, 2015.

[7] Hui-Shen Shen. Thermal postbuckling behavior of shear deformable fgm plates with temperature-dependent properties. *International Journal of Mechanical Sciences*, 49(4):466–478, 2007.

[8] Weikai Li and Baohong Han. Research and application of functionally gradient materials. In *IOP Conference Series: Materials Science and Engineering*, volume 394, page 022065. IOP Publishing, 2018.

[9] Rasheedat M Mahamood, Esther T Akinlabi, Mukul Shukla, and Sisa Pityana. Functionally graded material: An overview. In *Proceedings of the World Congress on Engineering*, volume 3, 2012.

[10] RK Rajput. *A textbook of manufacturing technology: Manufacturing processes*. Firewall Media, 2007.

[11] B Kieback, A Neubrand, and H Riedel. Processing techniques for functionally graded materials. *Materials Science and Engineering: A*, 362(1-2):81–106, 2003.

[12] S Uemura. The activities of fgm on new application. In *Materials Science Forum*, volume 423, pages 1–10. Trans Tech Publ, 2003.

[13] Marco Petrolo, Erasmo Carrera, Maria Cinefra, and Enrico Zappino. *Finite element analysis of structures through unified formulation*. John Wiley & Sons, 2014.

[14] Chuh Mei and Charles C Gray. Finite element analysis of thermal post-buckling and vibrations of thermally buckled composite plates. page 1239, 1991.

[15] Jeng-Shian Chang and Shyue-Ywh Leu. Thermal buckling analysis of antisymmetric angle-ply laminates based on a higher-order displacement field. *Composites science and technology*, 41(2):109–128, 1991.

[16] WJ Chen, PD Lin, and LW Chen. Thermal buckling behavior of thick composite laminated plates under nonuniform temperature distribution. *Computers & Structures*, 41(4):637–645, 1991.

[17] Lien-Wen Chen and Lei-Yi Chen. Thermal postbuckling behaviors of laminated composite plates with temperature-dependent properties. *Composite structures*, 19(3):267–283, 1991.

[18] Earl A Thornton. Thermal buckling of plates and shells. *Appl Mech Rev*, 46(10):485, 1993.

[19] MR Prabhu and R Dhanaraj. Thermal buckling of laminated composite plates. *Computers & structures*, 53(5):1193–1204, 1994.

[20] Hui-Shen Shen. Thermal post-buckling analysis of imperfect laminated plates using a higher-order shear deformation theory. *International journal of nonlinear mechanics*, 32(6):1035–1050, 1997.

[21] Maloy K Singha, LS Ramachandra, and JN Bandyopadhyay. Thermal postbuckling analysis of laminated composite plates. *Composite Structures*, 54(4):453–458, 2001.

[22] R Javaheri and MR Eslami. Thermal buckling of functionally graded plates. *AIAA journal*, 40(1):162–169, 2002.

[23] R Javaheri and MR Eslami. Thermal buckling of functionally graded plates based on higher order theory. *Journal of thermal stresses*, 25(7):603–625, 2002.

[24] KM Liew, Jie Yang, and Sritawat Kitipornchai. Thermal post-buckling of laminated plates comprising functionally graded materials with temperature-dependent properties. *J. Appl. Mech.*, 71(6):839–850, 2004.

[25] Wu Lanhe. Thermal buckling of a simply supported moderately thick rectangular fgm plate. *Composite Structures*, 64(2):211–218, 2004.

[26] BA Samsam Shariat and MR Eslami. Thermal buckling of imperfect functionally graded plates. *International journal of solids and structures*, 43(14-15):4082–4096, 2006.

[27] BA Samsam Shariat and MR Eslami. Thermomechanical stability of imperfect functionally graded plates based on the third order theory. *AIAA journal*, 44(12):2929–2936, 2006.

[28] BA Samsam Shariat and MR Eslami. Buckling of thick functionally graded plates under mechanical and thermal loads. *Composite Structures*, 78(3):433–439, 2007.

[29] SA Hosseini Kordkheili and R Naghdabadi. Geometrically non-linear thermoelastic analysis of functionally graded shells using finite element method. *International journal for numerical methods in Engineering*, 72(8):964–986, 2007.

[30] NS Viliani, SMR Khalili, and H Porrostami. Buckling analysis of fg plate with smart sensor/actuator. 2009.

[31] AM Zenkour and M Sobhy. Thermal buckling of various types of fgm sandwich plates. *Composite Structures*, 93(1):93–102, 2010.

[32] Y Mohammadi and SMR Khalili. Free vibration analysis of sandwich plates with temperature-dependent properties of the core materials and functionally graded face sheets. *Mechanics and Properties of Composed Materials and Structures*, pages 183–197, 2012.

[33] Fiorenzo Adolfo Fazzolari and Erasmo Carrera. Advanced variable kinematics ritz and galerkin formulations for accurate buckling and vibration analysis of anisotropic laminated composite plates. *Composite Structures*, 94(1):50–67, 2011.

[34] F Fazzolari. Fully coupled thermo-mechanical effect in free vibration analysis of anisotropic multilayered plates by combining hierarchical plate models and a trigonometric ritz formulation. 2012.

[35] Fiorenzo Adolfo Fazzolari and Erasmo Carrera. Thermo-mechanical buckling analysis of anisotropic multilayered composite and sandwich plates by using refined variable-kinematics theories. *Journal of Thermal Stresses*, 36(4):321–350, 2013.

[36] Fiorenzo A Fazzolari and Erasmo Carrera. Accurate free vibration analysis of thermo-mechanically pre/post-buckled anisotropic multilayered plates based on a refined hierarchical trigonometric ritz formulation. *Composite Structures*, 95:381–402, 2013.

[37] Fiorenzo A Fazzolari and Erasmo Carrera. Free vibration analysis of sandwich plates with anisotropic face sheets in thermal environment by using the hierarchical trigonometric ritz formulation. *Composites Part B: Engineering*, 50:67–81, 2013.

[38] Fiorenzo A Fazzolari and Erasmo Carrera. Advances in the ritz formulation for free vibration response of doubly-curved anisotropic laminated composite shallow and deep shells. *Composite Structures*, 101:111–128, 2013.

[39] FA Fazzolari and E Carrera. Thermal stability of fgm sandwich plates under various through-the-thickness temperature distributions. *Journal of Thermal Stresses*, 37(12):1449–1481, 2014.

[40] Fiorenzo A Fazzolari and Erasmo Carrera. Coupled thermoelastic effect in free vibration analysis of anisotropic multilayered plates and fgm plates by using a variable-kinematics ritz formulation. *European Journal of Mechanics-A/Solids*, 44:157–174, 2014.

[41] Otbi Bouguenina, Khalil Belakhdar, Abdelouahed Tounsi, and El Abbes Adda Bedia. Numerical analysis of fgm plates with variable thickness subjected to thermal buckling. *Steel Compos. Struct., Int. J*, 19(3):679–695, 2015.

[42] Young-Hoon Lee, Seok-In Bae, and Ji-Hwan Kim. Thermal buckling behavior of functionally graded plates based on neutral surface. *Composite Structures*, 137:208–214, 2016.

[43] Tiantang Yu, Shuohui Yin, Tinh Quoc Bui, Chen Liu, and Nuttawit Wattanasakulpong. Buckling isogeometric analysis of functionally graded plates under combined thermal and mechanical loads. *Composite Structures*, 162:54–69, 2017.

[44] Ahmed Amine Daikh and Abdelkader Megueni. Thermal buckling analysis of functionally graded sandwich plates. *Journal of Thermal Stresses*, 41(2):139–159, 2018.

[45] B Wu, A Pagani, M Filippi, WQ Chen, and E Carrera. Large-deflection and post-buckling analyses of isotropic rectangular plates by carrera unified formulation. *International Journal of Non-Linear Mechanics*, 116:18–31, 2019.

[46] Amira Sadgui and Abdelouahab Tati. A novel trigonometric shear deformation theory for the buckling and free vibration analysis of functionally graded plates. *Mechanics of Advanced Materials and Structures*, pages 1–16, 2021.

[47] Saeed I Tahir, Abdelbaki Chikh, Abdelouahed Tounsi, Mohammed A Al-Osta, Salah U Al-Dulaijan, and Mesfer M Al-Zahrani. Wave propagation analysis of a ceramic-metal functionally graded sandwich plate with different porosity distributions in a hygro-thermal environment. *Composite Structures*, 269:114030, 2021.

[48] Ismail M Mudhaffar, Abdelouahed Tounsi, Abdelbaki Chikh, Mohammed A Al-Osta, Mesfer M Al-Zahrani, and Salah U Al-Dulaijan. Hygro-thermo-mechanical bending behavior of advanced functionally graded ceramic metal plate resting on a viscoelastic foundation. In *Structures*, volume 33, pages 2177–2189. Elsevier, 2021.

[49] Mohamad W Zaitoun, Abdelbaki Chikh, Abdelouahed Tounsi, Mohammed A Al-Osta, Alfarabi Sharif, Salah U Al-Dulaijan, and Mesfer M Al-Zahrani. Influence of the visco-pasternak foundation parameters on the buckling behavior of a sandwich functional graded ceramic–metal plate in a hygrothermal environment. *Thin-Walled Structures*, 170:108549, 2022.

[50] Chennakesava Kadapa. A simple extrapolated predictor for overcoming the starting and tracking issues in the arc-length method for nonlinear structural mechanics. *Engineering Structures*, 234:111755, 2021.

[51] Mojtaba Farrokh, Majid Afzali, and Erasmo Carrera. Mechanical and thermal buckling loads of rectangular fg plates by using higher-order unified formulation. *Mechanics of Advanced Materials and Structures*, pages 1–10, 2019.

[52] Abderrahman Rachid, Djamel Ouinas, Abdelkader Lousdad, Fatima Zohra Zaoui, Belkacem Achour, Hatem Gasmi, Tayyab Ashfaq Butt, and Abdelouahed Tounsi. Mechanical behavior and free vibration analysis of fg doubly curved shells on elastic foundation via a new modified displacements field model of 2d and quasi-3d hsdts. *Thin-Walled Structures*, 172:108783, 2022.

[53] Sajedeh Khosravani, Mohammad Homayoune Sadr, Erasmo Carrera, and Alfonso Pagani. Synthesis, experimental testing and multi-scale modelling of graphene foam/epoxy composite. *Mechanics of Advanced Materials and Structures*, pages 1–10, 2022.

[54] Sajedeh Khosravani, Mohammad Homayoune Sadr, Erasmo Carrera, Alfonso Pagani, and Alberto Racionero Sanchez-Majano. Multi-scale analysis of thermoelastic properties of graphene foam/pdms composites. *Computational Materials Science*, 216:111842, 2023.

[55] Mojtaba Farrokh, Mohammad Taheripur, and Erasmo Carrera. Optimum distribution of materials for functionally graded rectangular plates considering thermal buckling. *Composite Structures*, page 115401, 2022.

[56] Ravi Kumar, Ajay Kumar, and Divesh Ranjan Kumar. Buckling response of cnt based hybrid fg plates using finite element method and machine learning method. *Composite Structures*, page 117204, 2023.

[57] Arash Tavakoli Maleki, Hadi Parviz, Akbar A Khatibi, and Mahnaz Zakeri. Probabilistic stability of uncertain composite plates and stochastic irregularity in their buckling mode shapes: A semi-analytical non-intrusive approach. *Frontiers of Structural and Civil Engineering*, 17(2):179–190, 2023.

[58] Xiuhua Chen, Hui-Shen Shen, and Y Xiang. Re-examination of thermo-mechanical buckling and postbuckling responses of sandwich plates with porous fg-gplrc core. *Thin-Walled Structures*, 187:110735, 2023.

[59] Di Wang, Jizhuang Hui, Wei Cao, Yu Yang, Yipin Wan, Hao Zuo, and Bo Zhang. The influence of geometric imperfections on post-buckling behavior and free vibrations of a fiber-reinforced composite laminated plate under thermal loading. *Composite Structures*, 306:116568, 2023.

[60] JN Reddy and CD Chin. Thermomechanical analysis of functionally graded cylinders and plates. *Journal of thermal Stresses*, 21(6):593–626, 1998.

[61] F Moleiro, JFA Madeira, E Carrera, and AJM Ferreira. Thermo-mechanical design optimization of symmetric and non-symmetric sandwich plates with ceramic-metal-ceramic functionally graded core to minimize stress, deformation and mass. *Composite Structures*, page 114496, 2021.

[62] E Carrera. A study on arc-length-type methods and their operation failures illustrated by a simple model. *Computers & structures*, 50(2):217–229, 1994.

[63] Carmen Campos and Jose E Roman. Nep: A module for the parallel solution of nonlinear eigenvalue problems in slepc. *ACM Transactions on Mathematical Software (TOMS)*, 47(3):1–29, 2021.

Appendix A

Appendix

A.1 Fundamental nucleus

FN of stiffness is a 3×3 matrix with nine components that include the below sub-matrices:

FN's components for the linear stiffness matrix $\mathbf{K}_0^{ij\tau s}[r,c]$ are stated as follows:

$$
\begin{aligned}
K_0^{ij\tau s}[1,1] &= \left\langle C_{11} F_\tau F_s N_{i,x} N_{j,x} \right\rangle + \left\langle C_{44} F_{\tau,z} F_{s,z} N_i N_j \right\rangle \\
&\quad + \left\langle C_{66} F_\tau F_s N_{i,y} N_{j,y} \right\rangle \\
K_0^{ij\tau s}[1,2] &= \left\langle C_{66} F_\tau F_s N_{i,y} N_{j,x} \right\rangle + \left\langle C_{12} F_\tau F_s N_{i,x} N_{j,y} \right\rangle \\
K_0^{ij\tau s}[1,3] &= \left\langle C_{13} F_\tau F_{s,z} N_{i,x} N_j \right\rangle + \left\langle C_{44} F_{\tau,z} F_s N_i N_{j,x} \right\rangle \\
K_0^{ij\tau s}[2,1] &= \left\langle C_{12} F_\tau F_s N_{i,y} N_{j,x} \right\rangle + \left\langle C_{66} F_\tau F_s N_{i,x} N_{j,y} \right\rangle \\
K_0^{ij\tau s}[2,2] &= \left\langle C_{66} F_\tau F_s N_{i,x} N_{j,x} \right\rangle + \left\langle C_{55} F_{\tau,z} F_{s,z} N_i N_j \right\rangle \\
&\quad + \left\langle C_{22} F_\tau F_s N_{i,y} N_{j,y} \right\rangle \\
K_0^{ij\tau s}[2,3] &= \left\langle C_{23} F_\tau F_{s,z} N_{i,y} N_j \right\rangle + \left\langle C_{55} F_{\tau,z} F_s N_i N_{j,y} \right\rangle \\
K_0^{ij\tau s}[3,1] &= \left\langle C_{44} F_\tau F_{s,z} N_{i,x} N_j \right\rangle + \left\langle C_{13} F_{\tau,z} F_s N_i N_{j,x} \right\rangle \\
K_0^{ij\tau s}[3,2] &= \left\langle C_{55} F_\tau F_{s,z} N_{i,y} N_j \right\rangle + \left\langle C_{23} F_{\tau,z} F_s N_i N_{j,y} \right\rangle \\
K_0^{ij\tau s}[3,3] &= \left\langle C_{44} F_\tau F_s N_{i,x} N_{j,x} \right\rangle + \left\langle C_{33} F_{\tau,z} F_{s,z} N_i N_j \right\rangle \\
&\quad + \left\langle C_{55} F_\tau F_s N_{i,y} N_{j,y} \right\rangle
\end{aligned}
$$

FN's components for the first-order nonlinear stiffness matrix $\mathbf{K}_{nll}^{ij\tau s}[r,c]$ are filled as below:

$$
\begin{aligned}
&For\ \ r = 1:3 \\
&K_{nll}^{ij\tau s}[r,1] = \left\langle \mathbf{u}_{,x}[r] C_{11} F_\tau F_s N_{i,x} N_{j,x} \right\rangle + \left\langle \mathbf{u}_{,x}[r] C_{44} F_{\tau,z} F_{s,z} N_i N_j \right\rangle \\
&\quad + \left\langle \mathbf{u}_{,x}[r] C_{66} F_\tau F_s N_{i,y} N_{j,y} \right\rangle + \left\langle \mathbf{u}_{,y}[r] C_{66} F_\tau F_s N_{i,x} N_{j,y} \right\rangle \\
&\quad + \left\langle \mathbf{u}_{,y}[r] C_{12} F_\tau F_s N_{i,y} N_{j,x} \right\rangle + \left\langle \mathbf{u}_{,z}[r] C_{44} F_\tau F_{s,z} N_{i,x} N_j \right\rangle \\
&\quad + \left\langle \mathbf{u}_{,z}[r] C_{13} F_{\tau,z} F_s N_i N_{j,x} \right\rangle \\
&K_{nll}^{ij\tau s}[r,2] = \left\langle \mathbf{u}_{,x}[r] C_{12} F_\tau F_s N_{i,x} N_{j,y} \right\rangle + \left\langle \mathbf{u}_{,x}[r] C_{66} F_\tau F_s N_{i,y} N_{j,x} \right\rangle \\
&\quad + \left\langle \mathbf{u}_{,y}[r] C_{66} F_\tau F_s N_{i,x} N_{j,x} \right\rangle + \left\langle \mathbf{u}_{,y}[r] C_{55} F_{\tau,z} F_{s,z} N_i N_j \right\rangle \\
&\quad + \left\langle \mathbf{u}_{,y}[r] C_{22} F_\tau F_s N_{i,y} N_{j,y} \right\rangle + \left\langle \mathbf{u}_{,z}[r] C_{23} F_{\tau,z} F_s N_i N_{j,y} \right\rangle \\
&\quad + \left\langle \mathbf{u}_{,z}[r] C_{55} F_\tau F_{s,z} N_{i,y} N_j \right\rangle \\
&K_{nll}^{ij\tau s}[r,3] = \left\langle \mathbf{u}_{,x}[r] C_{13} F_\tau F_{s,z} N_{i,x} N_j \right\rangle + \left\langle \mathbf{u}_{,x}[r] C_{44} F_{\tau,z} F_s N_i N_{j,x} \right\rangle \\
&\quad + \left\langle \mathbf{u}_{,y}[r] C_{55} F_{\tau,z} F_s N_i N_{j,y} \right\rangle + \left\langle \mathbf{u}_{,y}[r] C_{23} F_\tau F_{s,z} N_{i,y} N_j \right\rangle \\
&\quad + \left\langle \mathbf{u}_{,z}[r] C_{44} F_\tau F_s N_{i,x} N_{j,x} \right\rangle + \left\langle \mathbf{u}_{,z}[r] C_{33} F_{\tau,z} F_{s,z} N_i N_j \right\rangle \\
&\quad + \left\langle \mathbf{u}_{,z}[r] C_{55} F_\tau F_s N_{i,y} N_{j,y} \right\rangle \\
&end
\end{aligned}
$$

It should be noted that $\mathbf{K}_{lnl}^{ij\tau s} = (\mathbf{K}_{nll}^{ij\tau s})^T$.

FN's components for the second-order nonlinear stiffness matrix $\mathbf{K}_{nlnl}^{ij\tau s}[r,c]$ are made as:

$$
\begin{aligned}
&\textit{For}\ \ r = 1:3\\
&\quad \textit{For}\ \ c = 1:3\\
&\\
&2\times K_{nlnl}^{ij\tau s}[r,c] = \left\langle \mathbf{u}_{,x}[r]\mathbf{u}_{,x}[c]C_{11}F_{\tau}F_{s}N_{i,x}N_{j,x}\right\rangle\\
&\qquad\qquad + \left\langle \mathbf{u}_{,x}[r]\mathbf{u}_{,x}[c]C_{44}F_{\tau_{,z}}F_{s_{,z}}N_{i}N_{j}\right\rangle\\
&\qquad\qquad + \left\langle \mathbf{u}_{,x}[r]\mathbf{u}_{,x}[c]C_{66}F_{\tau}F_{s}N_{i,y}N_{j,y}\right\rangle\\
&\qquad\qquad + \left\langle \mathbf{u}_{,y}[r]\mathbf{u}_{,y}[c]C_{66}F_{\tau}F_{s}N_{i,x}N_{j,x}\right\rangle\\
&\qquad\qquad + \left\langle \mathbf{u}_{,y}[r]\mathbf{u}_{,y}[c]C_{55}F_{\tau_{,z}}F_{s_{,z}}N_{i}N_{j}\right\rangle\\
&\qquad\qquad + \left\langle \mathbf{u}_{,y}[r]\mathbf{u}_{,y}[c]C_{22}F_{\tau}F_{s}N_{i,y}N_{j,y}\right\rangle\\
&\qquad\qquad + \left\langle \mathbf{u}_{,z}[r]\mathbf{u}_{,z}[c]C_{44}F_{\tau}F_{s}N_{i,x}N_{j,x}\right\rangle\\
&\qquad\qquad + \left\langle \mathbf{u}_{,z}[r]\mathbf{u}_{,z}[c]C_{33}F_{\tau_{,z}}F_{s_{,z}}N_{i}N_{j}\right\rangle\\
&\qquad\qquad + \left\langle \mathbf{u}_{,z}[r]\mathbf{u}_{,z}[c]C_{55}F_{\tau}F_{s}N_{i,y}N_{j,x}\right\rangle\\
&\qquad\qquad + \left\langle \mathbf{u}_{,x}[r]\mathbf{u}_{,y}[c]C_{12}F_{\tau}F_{s}N_{i,x}N_{j,y}\right\rangle\\
&\qquad\qquad + \left\langle \mathbf{u}_{,x}[r]\mathbf{u}_{,y}[c]C_{66}F_{\tau}F_{s}N_{i,y}N_{j,x}\right\rangle\\
&\qquad\qquad + \left\langle \mathbf{u}_{,y}[r]\mathbf{u}_{,x}[c]C_{12}F_{\tau}F_{s}N_{i,y}N_{j,x}\right\rangle\\
&\qquad\qquad + \left\langle \mathbf{u}_{,y}[r]\mathbf{u}_{,x}[c]C_{66}F_{\tau}F_{s}N_{i,x}N_{j,y}\right\rangle\\
&\qquad\qquad + \left\langle \mathbf{u}_{,x}[r]\mathbf{u}_{,z}[c]C_{13}F_{\tau}F_{s_{,z}}N_{i,x}N_{j}\right\rangle\\
&\qquad\qquad + \left\langle \mathbf{u}_{,x}[r]\mathbf{u}_{,z}[c]C_{44}F_{\tau_{,z}}F_{s}N_{i}N_{j,x}\right\rangle\\
&\qquad\qquad + \left\langle \mathbf{u}_{,z}[r]\mathbf{u}_{,x}[c]C_{13}F_{\tau_{,z}}F_{s}N_{i}N_{j,x}\right\rangle\\
&\qquad\qquad + \left\langle \mathbf{u}_{,z}[r]\mathbf{u}_{,x}[c]C_{44}F_{\tau}F_{s_{,z}}N_{i,x}N_{j}\right\rangle\\
&\qquad\qquad + \left\langle \mathbf{u}_{,y}[r]\mathbf{u}_{,z}[c]C_{23}F_{\tau}F_{s_{,z}}N_{i,y}N_{j}\right\rangle\\
&\qquad\qquad + \left\langle \mathbf{u}_{,y}[r]\mathbf{u}_{,z}[c]C_{55}F_{\tau_{,z}}F_{s}N_{i}N_{j,y}\right\rangle\\
&\qquad\qquad + \left\langle \mathbf{u}_{,z}[r]\mathbf{u}_{,y}[c]C_{55}F_{\tau}F_{s_{,z}}N_{i,y}N_{j}\right\rangle\\
&\qquad\qquad + \left\langle \mathbf{u}_{,z}[r]\mathbf{u}_{,y}[c]C_{23}F_{\tau_{,z}}F_{s}N_{i}N_{j,y}\right\rangle\\
&\quad \textit{end}\\
&\textit{end}
\end{aligned}
$$

In the above formulations, $<\bigcirc>=\int \bigcirc dV$, where V is the volume of the plate. Also $\mathbf{u}_{,x}[\bigcirc]$, $\mathbf{u}_{,y}[\bigcirc]$ and $\mathbf{u}_{,z}[\bigcirc]$ represent the $\bigcirc^{th}$ component of the vector $\frac{\partial \mathbf{u}}{\partial x}$, $\frac{\partial \mathbf{u}}{\partial y}$ and $\frac{\partial \mathbf{u}}{\partial z}$ respectively, (e.g. $\mathbf{u}_{,x}[2] = u_{y,x}$).